

**SUB-PIXEL CLASSIFICATION OF URBAN AREA
USING FRACTION IMAGES FROM
MULTI-ENDMEMBER SPECTRAL ANALYSIS:
AMPHOE MUANG NAKHON RATCHASIMA**

Chotipa Kulrat

**A Thesis Submitted in Fulfillment of the Requirements for the
Degree of Master of Science in Geoinformatics
Suranaree University of Technology
Academic Year 2008**

การจำแนกพื้นที่ชุมชนในระดับรายละเอียดสูงกว่าจุดภาพ โดยใช้ข้อมูลภาพ
ตัดส่วนจากการวิเคราะห์เชิงรังสีหลายเอ็นด์เมมเบอร์: อำเภอเมืองนครราชสีมา

นางสาวโชติภา กุศลรัตน์

วิทยานิพนธ์นี้เป็นส่วนหนึ่งของการศึกษาตามหลักสูตรปริญญาวิทยาศาสตรมหาบัณฑิต
สาขาวิชาภูมิสารสนเทศ
มหาวิทยาลัยเทคโนโลยีสุรนารี
ปีการศึกษา 2551

**SUB-PIXEL CLASSIFICATION OF URBAN AREA USING
FRACTION IMAGES FROM MULTI-ENDMEMBER SPECTRAL
ANALYSIS: AMPHOE MUANG NAKHON RATCHASIMA**

Suranaree University of Technology has approved this thesis submitted in fulfillment of the requirements for a Master's Degree.

Thesis Examining Committee

(Assoc. Prof. Dr. Prapan Manyum)

Chairperson

(Asst. Prof. Dr. Sunya Sarapirome)

Member (Thesis Advisor)

(Asst. Prof. Dr. Songkot Dasananda)

Member

(Dr. Suwit Ongsomwang)

Member

(Prof. Dr. Pirote Sattayatham)

Vice Rector for Academic Affairs

(Assoc. Prof. Dr. Prapan Manyum)

Dean of Institute of Science

โชติภา กุศลรัตน์ : การจำแนกพื้นที่ชุมชนในระดับรายละเอียดสูงกว่าจุดภาพ โดยใช้ข้อมูลภาพสัดส่วนจากการวิเคราะห์เชิงรังสีหลายเอนด์เมมเบอร์: อำเภอเมืองนครราชสีมา (SUB-PIXEL CLASSIFICATION OF URBAN AREA USING FRACTION IMAGES FROM MULTI-ENDMEMBER SPECTRAL ANALYSIS: AMPHOE MUANG NAKHON RATCHASIMA) อาจารย์ที่ปรึกษา : ผู้ช่วยศาสตราจารย์ ดร.สัญญา สราภิรมย์, 82 หน้า

การวิจัยมีวัตถุประสงค์เพื่อทำการเปรียบเทียบความถูกต้องในการจำแนกการใช้ประโยชน์ที่ดินและสิ่งปกคลุมดินในพื้นที่ชุมชน อำเภอเมือง จังหวัดนครราชสีมาโดยใช้ข้อมูลภาพและวิธีการที่ต่างกันไป ข้อมูลภาพสัดส่วน (fraction images) ของเอนด์เมมเบอร์ 4 ชนิด ครอบคลุมถึง พืชพรรณ สิ่งปลูกสร้าง ดิน และ เงาม ถูกสร้างขึ้นโดยใช้วิธีการวิเคราะห์รังสีผสมเชิงเส้นซึ่งใช้ค่าลายเซ็นเชิงคลื่นของเอนด์เมมเบอร์ที่สกัดจากระบวนการแปลงรูป PCA จากข้อมูลภาพ TM ผลลัพธ์ได้เป็นข้อมูลภาพสัดส่วนสองชุดได้แก่ พืชพรรณ-สิ่งปลูกสร้าง-ดิน (V-I-S) และ พืชพรรณ-ดิน-เงา (V-S-Sh) ซึ่งถูกนำไปใช้ในการจำแนกด้วยวิธี MLC และ EMC ในขณะที่ข้อมูลภาพ TM ถูกใช้ในการจำแนกด้วยวิธี MLC ผลจากการจำแนกได้เป็นแผนที่แสดงการใช้ประโยชน์ที่ดินและสิ่งปกคลุมดิน 5 ชนิด ซึ่งได้รับการประเมินความถูกต้องโดยใช้ตารางประเมินค่าความคลาดเคลื่อน (error matrix) ผลการประเมินแสดงว่าแผนที่ที่ทำการจำแนกจากข้อมูลภาพสัดส่วนทั้งหมดมีความถูกต้องและค่าสถิติค่าปรับสูงกว่าแผนที่ที่จำแนกจากข้อมูลภาพ TM การจำแนกข้อมูลภาพสัดส่วน V-I-S ด้วยวิธี MLC จะให้ความถูกต้องโดยรวมสูงสุด (72.21%) และการจำแนกข้อมูลภาพ TM ด้วยวิธี MLC จะให้ความถูกต้องโดยรวมต่ำสุด (66.93%) ค่าความถูกต้องบนพื้นฐานของ producer และ user ของประเภทจำแนกต่างๆ ที่เป็นผลจากการใช้ข้อมูลภาพและวิธีการที่ต่างกันจะได้รับการรายงานและพิจารณาเช่นกัน

สาขาวิชาการรับรู้จากระยะไกล

ปีการศึกษา 2551

ลายมือชื่อนักศึกษา _____

ลายมือชื่ออาจารย์ที่ปรึกษา _____

CHOTIPA KULRAT : SUB-PIXEL CLASSIFICATION OF URBAN AREA
USING FRACTION IMAGES FROM MULTI-ENDMEMBER SPECTRAL
ANALYSIS: AMPHOE MUANG NAKHON RATCHASIMA. THESIS
ADVISOR : ASST. PROF. SUNYA SARAPIROME, Ph.D. 82 PP.

SMA/LSMA/ENDMEMBER/FRACTION IMAGES/ENDMEMBER MODEL
CLASSIFICATION/NAKHON RATCHASIMA

The objective of this research is to compare accuracies of urban LULC classification of Muang District, Nakhon Ratchasima Province using different types of images and methods. Fraction images of four endmembers covering green vegetation, impervious surface, soil, and shade are generated using LSMA with input of their spectral signatures extracted from scatter-plot of PCA transformation of TM images. This results in two sets of fraction images i.e. V-I-S and V-S-Sh. These two sets of fraction images are classified by Maximum Likelihood Classification (MLC) and Endmember Model Classification (EMC) methods while original TM images are classified by MLC. Accuracies of five resulting LULC maps of the study area are assessed using error matrix. The assessment reveals that all maps derived from fraction images show higher overall accuracy and Kappa statistics than the one from original TM images. MLC of V-I-S provides highest overall accuracy (72.21%) and MLC of original TM provides lowest overall accuracy (66.93%). Accuracies of LULC classes from different methods and images based on producer's and user's accuracies are also reported and discussed.

School of Remote Sensing

Academic Year 2008

Student's Signature_____

Advisor's Signature_____

ACKNOWLEDGEMENTS

I wish to express my deep gratitude to my thesis advisor, Asst. Prof. Dr. Sunya Sarapirome, who gave valuable advises throughout the thesis, making suggestion and comments, reading drafts for improving the thesis.

I would like to express my appreciations to all members of thesis examination committee, Assoc. Prof. Dr. Prapan Manyum, Asst. Prof. Dr. Sunya Sarapirome, Asst. Prof. Dr. Songkot Dasananda, and Dr. Suwit Ongsomwang.

I would like to thanks to the GISTDA in providing Landsat5 TM data used in the thesis. Research budget partially supported by Suranaree University of Technology is also greatly appreciated.

Finally, I would like to thank my family members for their understanding and moral support during the years of my study.

Chotipa Kulrat

CONTENTS

	Page
ABSTRACT IN THAI	I
ABSTRACT IN ENGLISH.....	II
ACKNOWLEDGEMENTS.....	III
CONTENTS.....	IV
LIST OF TABLES.....	VII
LIST OF FIGURES.....	X
LIST OF ABBREVIATIONS.....	XII
 CHAPTER	
I INTRODUCTION.....	1
1.1 Significance of the Study.....	1
1.2 Research Objectives.....	3
1.3 Research Hypothesis.....	3
1.4 Definition.....	3
1.5 Scope and Limitations of the Study.....	4
1.6 Study Area.....	5
1.7 Expected Results.....	6
II LITERATURE REVIEW.....	7
2.1 Conventional Methods.....	7
2.2 Linear Spectral Mixture Analysis.....	9
III RESEARCH PROCEDURE.....	18

CONTENTS (Continued)

	Page
5.3.2 Fraction image classification.....	40
5.3.2.1 Maximum likelihood classification.....	40
1) V-I-S fraction images.....	40
2) V-S-Sh fraction images.....	42
5.3.2.2 Endmember model classification.....	43
1) V-I-S fraction images.....	44
2) V-S-Sh fraction images.....	46
5.4 Accuracy Assessments.....	49
5.4.1 Accuracy assessments of MLC.....	52
1) Original Landsat5 TM images.....	52
2) V-I-S fraction images.....	53
3) V-S-Sh fraction images.....	55
5.4.2 Accuracy assessments of EMC.....	56
1) V-I-S fraction images.....	56
2) V-S-Sh fraction images.....	58
VI CONCLUSION AND DISCUSSION.....	60
6.1 Conclusion.....	60
6.2 Discussion.....	64
REFERENCES.....	68
APPENDIX.....	75
CURRICULUM VITAE.....	82

LIST OF TABLES

Table	Page
2.1 The classification conditions used to classify land cover in Brazilian Amazon forest (Adams et al., 1995).....	11
3.1 Summarized methods used for data analysis.....	23
4.1 The statistical data of the 2 nd order polynomial model for image rectification.....	29
4.2 The transformation parameters of rectification.....	30
5.1 Pixel number and area of each class classified using MLC for original Landsat5 TM images.....	39
5.2 Number of pixels and area classified for each class of MLC for V-I-S fraction images.....	41
5.3 Number of pixels and area classified for each class of MLC for V-S-Sh fraction images.....	43
5.4 The definition of LULC types classified for V-I-S fraction images using endmember model.....	44
5.5 Number of pixels and area for each class of V-I-S fraction images using endmember model.....	45
5.6 The definition of LULC types classified for V-S-Sh fraction images.....	47
5.7 Number of pixels and area for each class of V-S-Sh fraction images using endmember model.....	47

LIST OF TABLES (Continued)

Table	Page
5.8 Total number of samples and number of samples per class used for accuracy determinations.....	51
5.9 Error matrix of the LULC map derived from MLC of original Landsat5 TM images.....	52
5.10 Producer's and user's accuracies the LULC map derived from MLC of original Landsat5 TM images.....	53
5.11 Error matrix of the LULC map derived from MLC of V-I-S fraction images.....	54
5.12 The producer's and user's accuracies of the LULC map derived from MLC of V-I-S fraction images.....	54
5.13 Error matrix of the LULC map derived from MLC of V-S-Sh fraction images.....	55
5.14 The producer's and user's accuracies of the LULC map derived from MLC of V-S-Sh fraction images.....	56
5.15 Error matrix of the land-use map derived from EMC of V-I-S fraction images.....	57
5.16 The producer's and user's accuracies of the land-used map derived from EMC of V-I-S fraction images.....	57
5.17 Error matrix of the classification map derived from EMC of V-S-Sh fraction images.....	58

LIST OF TABLES (Continued)

Table	Page
5.18 The producer's and user's accuracies of the LULC map derived from EMC of V-S-Sh fraction images.....	59
6.1 Summarized a percentage of each classified LULC class from each map of different classification methods.....	62
6.2 Summarized overall accuracy and overall Kappa statistics of each map classified using different sets of images and methods.....	62
6.3 Summarized the PA and UA of each LULC class for all classification methods.....	63

LIST OF FIGURES

Figure	Page
1.1 Study area is Amphoe Muang Nakhon Ratchasima urban area.....	5
2.1 Relationship of green vegetation fraction, NDVI, and built up fraction with the field measurements of impervious surface (Matthias and Martin, 2003)....	14
2.2 A Lu-Weng conceptual model (Lu and Weng, 2004).....	16
3.1 Flow chart of the research procedure.....	19
3.2 Flow chart of LSMA method.....	20
4.1 Landsat5 TM images, displayed in false colors composite with RGB: 432 covering Nakhon Ratchasima province.....	26
4.2 The 21 mosaic scenes of aerial photograph were used as reference image for Landsat5 TM rectification.....	27
4.3 Landsat5 TM covering Muang Nakhon Ratchasima municipal with the twenty five reference points from color aerial photographs, displayed in false colors composite with RGB: 453.....	28
4.4 Comparison of the rectified image (a) and the original image (b) of TM5 covering study area, displayed in false colors with RGB: 453.....	29
5.1 Training sites selection for the classifications.....	32
5.2 Photos showing CBD (a), residential area (b), grass field (c), horticultural area (d), paddy field (e), and shrub (f) of Nakhon Ratchasima municipality...	33
5.3 PC1, PC2, and PC3 images of study area.....	34

LIST OF FIGURES (Continued)

Figure	Page
5.4 Scatter-plots of principal component images for municipal area: a) the plot of PC1 and PC2, b) the plot of PC1 and PC3, and c) the plot of PC2 and PC3.....	35
5.5 Shows the green vegetation, impervious surface, bare soil, and RMSE fraction images of the study area.....	37
5.6 Shows the green vegetation, bare soil, shade, and RMSE fraction images of the study area.....	38
5.7 LULC map by MLC for original Landsat5 TM images.....	39
5.8 LULC map by MLC for V-I-S fraction images.....	41
5.9 LULC map by MLC for V-S-Sh fraction images.....	42
5.10 Ternary diagram of green vegetation, impervious surface, and soil (V-I-S) fractions of the study area.....	45
5.11 LULC map by EMC of V-I-S fraction images.....	46
5.12 Ternary diagram of green vegetation, soil, and shade fractions (V-S-Sh) of the study area.....	48
5.13 LULC map by EMC of V-S-Sh fraction images.....	49
A1 Flow diagram of fractions image generation using LSMA.....	77
A2 A scatter-plot of band i and band j, a unique reflectance signature of the pure ground component will locate at extremes of triangle in the feature space. (Plaza et al., 2002).....	79

LIST OF ABBREVIATIONS

SMA	=	Spectral Mixture Analysis
LSMA	=	Linear Spectral Mixture Analysis
NLSMA	=	Non Linear Spectral Mixture Analysis
MLC	=	Maximum Likelihood Classification
MDMC	=	Minimum Distance to Mean Classification
EMC	=	Endmember Model Classification
PCA	=	Principal Component Analysis
MNF	=	Minimum Noise Fraction
PPI	=	Pixel Purity Index
LULC	=	Land Use and Land Cover
V-I-S	=	Vegetation-Impervious surface-Soil
V-S-Sh	=	Vegetation-Soil-Shade
NDVI	=	Normalized Differenced Vegetation Index
CBD	=	Central Business District
TM	=	Thematic Mapper
ETM+	=	Enhance Thematic Mapper Plus
USFS	=	United State Forest Service
AOI	=	Area of Interest
RMSE	=	Root Mean Square Error
PA	=	Producer's accuracy

LIST OF ABBREVIATIONS (Continued)

UA	=	User's accuracy
G/B	=	Grass field/Bare soil
GIFOV	=	Ground Instantaneous Field of View
MESM	=	Manual Endmember Selection Methods

CHAPTER I

INTRODUCTION

1.1 Significance of the Study

Urban areas have been grown constantly and rapidly due to economic and population growth. The growth adversely affect surrounding environment such as air pollution, sound pollution, traffic jam, and quality of life degradation. Therefore, study of urban change is considered important information to managing and planning a future development.

Remote sensing technology is a potential tool for monitoring the urban change dynamically. In general, a high spatial resolution remote sensing data such as QuickBird, IKONOS, and aerial photographs have been used because of the spatial complexity of components in the urban area such as building, road, runway, concrete, asphalt, and soil. The small urban component cannot be detected in the low-to-medium-spatial resolution data and it can mix with other component within a pixel. Since high spatial resolution data are costly, therefore, many researches are still concentrated on improving the classification accuracy using medium-spatial resolution remote sensing data, e.g. Landsat Thematic Mapper (TM) and Enhance Thematic Mapper plus (ETM+). Unfortunately, researches consider them in a pixel level which is too coarse to separate each component in an urban environment (Lu and Weng, 2004). The traditional classification approaches such as Maximum Likelihood Classification (MLC) and Minimum Distance to Mean Classification

(MDMC) are assumed that in an image pixel has only one land-use and land-cover (LULC) class. Due to the combination complexity in one image pixel of an urban or sub urban area, a spectral reflectance of a pixel may represent the combination of several land-use types as called a mixed pixel (Wu, 2004). A mixed pixel can be a problem effect to LULC classification accuracy.

Spectral Mixture Analysis (SMA) is an approach for multispectral and hyperspectral classification which extracts information from sub-pixel scale (Plaza, 2002). SMA model shows a relationship between spectral reflectance of a mixed pixel and the fractions of endmembers in a mixed pixel. These fractions can be vegetation, impervious surface, soil, and shade etc. SMA can be classified into Linear Spectral Mixture Analysis (LSMA) and Non-Linear Spectral Mixture Analysis (NLSMA) according to the complexity of the energy scattering. If photons reflect as a single scattering, the mixing can be modeled as a linear sum of a spectral reflectance of each component multiplied by its fraction covering in the pixel. If photon interacts with multiple scatterings such as multiple near-infrared scattering of dense vegetation, a non-linear spectral model should be applied (Wu and Murray, 2003). Some researchers use the Gaussian mixture analysis to model a multiple scattering of forest. However in most urban application, a multiple scattering may assumed to be negligible. For this research the LSMA will be used to improve the classification accuracy.

Amphoe Muang Nakhon Ratchasima urban area is chosen to be the study area because the area is being a fast-growing area with rapid population growth and could be the typically urban land-use pattern found in fast-growing areas in the northeast of Thailand which are different from other regions of the country. Urban and sub-urban

areas could be found in the municipal area, sub-urban and sub-rural found in outer municipal area. To improve classification accuracy, LSMA would be appropriate technique for fraction images generation which are further used in LULC classification using MLC and endmember model classification (EMC). Error matrix is applied to evaluate accuracy of results from different methods.

1.2 Research Objectives

1. To apply LSMA technique to generate fraction images for LULC classification using MLC and EMC.

2. To evaluate and compare statistically the accuracies of LULC classifications using MLC and EMC with LSMA fraction images and MLC with TM images.

1.3 Research Hypothesis

The accuracy of urban LULC classification in Amphoe Muang Nakhon Ratchasima using LSMA fraction images is higher than using TM images.

1.4 Definition

SMA (Spectral Mixture Analysis) is a model that spectral reflectance of each pixel is assumed as a combination of endmember reflectance.

LSMA (Linear Spectral Mixture Analysis) is a model that spectral reflectance of each pixel is assume as a linear combination of endmember reflectance.

Endmember is a unique spectral signature of the certain component of ground materials.

MLC (Maximum Likelihood Classification) is a classification using decision rule based on a probability that a pixel belongs to a particular class (Leica, 2002).

EMC (Endmember Model Classification) is a classification method used to classify fraction images based on threshold range of composition acquired from ternary plot.

RMSE (Root Mean Square Error) is a method to measure how well a specific calculated solution fits the original data. For the observation of phenomenon, a variation can be computed between the actual observation and a calculated value (Leica, 2002).

Accuracy assessment is the comparison of a classification to geographical data that is assumed to be true. Usually, the assumed true data are derived from ground truth (Leica, 2002).

1.5 Scope and Limitation of the Study

The medium spatial resolution remote sensing data ($25 \times 25 \text{ m}^2$ a pixel) as Landsat5 TM imagery acquired in 6 March 2005 on dry season are used to classify urban LULC in Amphoe Muang Nakhon Ratchasima urban area. Classification accuracies of both LSMA and MLC are computed using the error matrix and Kappa statistics. Aerial photographs with high-spatial resolution taken in year 2002 and field check data are used as references in error matrix. Eight classes of LULC will be classified including central business district (CBD), residential area, crop field, paddy field, grass field/bare soil, forest, and water. For each LULC class, multinomial distribution function is used to specify number of reference points and the stratified

random point function is used to pick the control points according to the number calculate from multinomial distribution function for the accuracy assessment.

1.6 Study Area

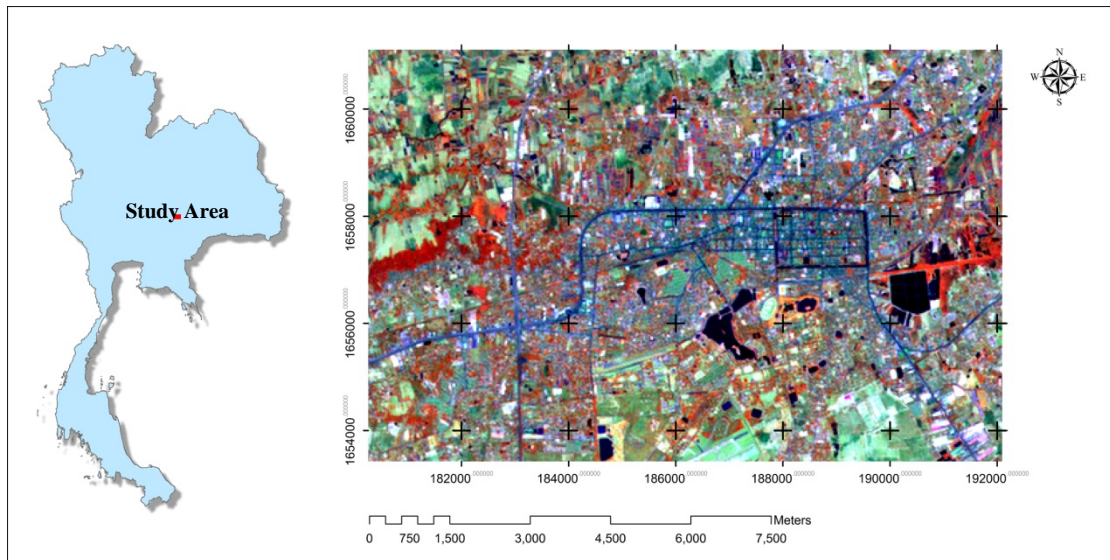


Figure 1.1 Study area is Amphoe Muang Nakhon Ratchasima urban area.

Amphoe Muang Nakhon Ratchasima urban area (Figure 1.1), located in northeast of Thailand, was selected as the study area. It has an area about 95 Km² covering a CBD, low and medium density residential and partly agricultural area. Its typical urban land-use pattern could be found in any fast-growing provinces in the northeast or elsewhere in Thailand. Nakhon Ratchasima province is the spatially largest and the second biggest population province of Thailand and is considered as the front door to the Northeast. Amphoe Muang Nakhon Ratchasima has encountered rapid urban environment and population growth. Around 20% of the municipal area is covered by CBD, low and medium density residential, and some agricultural area such as vegetable patch. Other 80% of outer areas are low density residential, agricultural area such as paddy field and horticultural area, some forest, bare soil and

some shrub. Accurate land-use classification particularly in the urban area can assist in monitoring urban expansion of Amphoe Muang Nakhon Ratchasima and controlling or planning its future development.

1.7 Expected Results

1. The LULC maps of the study area using MLC and EMC with LSMA fraction images and TM images.
2. The accuracy comparison of those LULC maps in terms of statistics.
3. Advantage and disadvantage of techniques used and suggestions how to achieve better result.

CHAPTER II

LITERATURE REVIEW

In this chapter, relevant literatures covering previous works on urban LULC classification methods are reviewed. They are related to applications of traditional methods to LULC classification, LSMA which include endmember selection and fraction images generation. These fraction images are further used with varying methods of LULC classification.

2.1 Conventional Methods

In traditional, visual interpretation has been used to interpret LULC from satellite data. The visual interpretation needs an experienced interpreter to analyze and extract information from sensor. Limitations of visual interpretation are time consuming, lack of experienced interpreter, and need of high spatial resolution data especially in urban area analysis. Therefore, the automate classification such as supervise and unsupervised classifications were lately replaced. These methods have been used for several decades. Details of their concepts and techniques used are generally mentioned in many well-known remote sensing books such as Jensen (2005) and some articles such as Yuan et al. (2005), Kaya and Curran (2006), and Han et al. (2004). They have been applied chiefly for TM data which are considered medium-resolution remotely sensed data.

In fact, within urban and sub-urban areas, there exists, apart from scattered vegetation cover, a complex combination of material such as building, concretes, road, asphalt, and soil. Some of this combination can actually be presented in only one pixel of the TM data. Therefore, in the complex combination area, the spectral reflectance of a pixel may represent a combination of several land-use types (Wu, 2004). This explains why using traditional methods result in low accuracy classification. High spatial resolution images can be used to solve this problem as mentioned by Chunfang, Kai, and Chonglong (2006), Weydahl, Bretar, and Bjerke (2005), and Cleve et al. (2008). Anyway, high spatial resolution image is still too costly. Therefore, more advanced method has been sought to improve classification accuracy when the same data are used, particularly in a heterogeneous area like urban. Lu and Weng (2004) reviewed previous methods used for improving urban LULC classification accuracy i.e. 1) use of advanced classifiers, for example fussy classification, ECHO classification, sub-pixel information extraction such as SMA (Friedl and Brodley, 1997; Zhu and Blumberg, 2002; and Kandrika and Roy, 2008), 2) incorporation of spectral and spatial information (Guindon, Zhang, and Dillabaugh, 2004; Dumas, Jappiot, and Tatoni, 2008), 3) incorporation of ancillary data such as TM with zoning data, housing densities, road densities, 4) use of multi-sensor data (Weydahl et al., 2005), 5) use of Normalized Difference Build-up Index (NDBI), 6) use of expert system (Jensen, 1997; and Stefanov, Ramsey, and Christensen, 2001), and 7) reclassification.

For this study, LSMA for fraction images generation and EMC are added on conventional methods and data.

2.2 Linear Spectral Mixture Analysis

SMA is an approach able to classify multi-spectral or hyper-spectral dataset by extract sub-pixel information because it shows a relationship between spectral reflectance of a mixed pixel and the endmember fractions in it. SMA was first reported in 1986 by Adams, Smith, and Johnson to analyst rock and soil type. It has been used for various applications e.g. 1) urban LULC classification (Lu and Weng, 2004; Lu and Weng, 2006; Powell et al., 2007; Wu and Murray, 2003; Wu, 2004; and Small, 2003), 2) measurement of vegetation abundance and distribution (Small and Lu, 2006; Weng, Lu, and Schubring, 2004; Small, 2001; Lu, Moran, and Betistella, 2003; and Defries, Hanson, and Townshend, 2002), 3) LULC change detection (Adams et al., 1995), 4) forest estimation (Sabol et al., 2002) and crop cover estimation (McNairn et al., 2001), and 5) snow cover estimation (Painter et al., 2003).

LSMA is the linear model of SMA that represents the spectral reflectance of each pixel of satellite data in terms of endmember and its fraction contain in the pixel. Endmember is a unique signature of a ground component. Assumption of the model is that every pixel is containing only three or four fundamental ground components. The original images will be transformed into fraction images by input the pure reflectance of a certain endmember to LSMA model (see LSMA equation in appendix A). The pure reflectance of an endmember can be extracted by various methods such as scatter-plot of principal component analysis (PCA) or minimum noise fraction (MNF) images, pixel purity index (PPI) function, measurement from laboratory, and spectral signature library, etc. A fraction image of a component indicates the percentage of the component containing in each pixel. Further, various methods can be applied to

classify the fraction images, for example, MLC and EMC such as vegetation-impervious surface-soil (V-I-S) of Ridd model or Lu and Weng conceptual model.

In 1990, LSMA was first applied to urban application by Ridd and Chung. After that in 1995, Ridd was the beginner to use the LSMA in form of the V-I-S model to present characteristic of urban/sub-urban environment. The following researches are some interesting examples of LSMA applications for LULC classification.

Adams et al. (1995) applied LSMA to four time spans of Landsat5 TM in years of 1988, 1989, 1990, and 1991 to monitoring land-cover change in Brazilian Amazon region. Four endmembers of shade, green vegetation, non-photosynthesis, and soil were collected by laboratory and field survey. After that gain and offset were combined to calibrate the endmember reflectance. Fraction images were produced by input the four endmembers into LSMA model. Training area of each land-cover class was selected and projected on the tetrahedral model to define the limit or land-cover definition of each land-cover class. The fraction images of four time spans were classified based on land-cover definitions in Table 2.1 and the temporal change of each class was analyzed and represented in the color composite image.

Small (2001) applied spectral mixture model to Landsat TM data for urban vegetation abundance estimation in New York City, USA. The MNF transformation was used to transform Landsat TM into MNF images. The three endmembers of high albedo, low albedo, and vegetation were selected from scatter-plot of the low order MNF images and input to LSMA equation to produce a three fraction images. Interpretation of color aerial photographs with two-meter resolution was used to

compare the vegetation fraction estimated from Landsat TM data. The radially symmetric TM point spread function was applied to aerial photographs and resulted in 50m x 50m GIFOV of aerial photographs. The vegetation fraction estimated from Landsat TM was compared with 50m x 50m GIFOV of aerial photographs. The results indicated that vegetation abundance measured from aerial photographs showed agreement with vegetation fraction image derived from Landsat TM.

Table 2.1 The classification conditions used to classify land cover in Brazilian Amazon forest (Adams et al., 1995)

category number	Class Name	Description/comment
1	Primary forest	High shade, 30-80% NPV, no detectable soil.
	Mature re-growth forest	
	Burned fields, partly vegetated	High shade, 30-80% NPV, no detectable soil.
2	Closed-canopy re-growth	Low shade, <30% NPV, no detectable soil.
	Kudzu vine (or Crops)	Very low shade, <30% NPV, no crops in study area.
3	Open canopy re-growth	Low shade, <30% NPV, soil detectable but <30% exposed.
4	Pasture	Moderate shade; high shade for tall, upright grass: 30-80% NPV; <30% soil.
	Crops	Very low to moderate shade, 30-80% NPV, <30% soil.
5	Sparse cleared slash	Low shade, >30% exposed soil, 0-70% NPV.
	Partially cleared slash	Low shade, >30% soil, 0-70% NPV.
	Partially burned slash	Low to high shade, >30% soil, 0-70% NPV.
6	Dry pasture	Low shade, >50% NPV, <30% soil.
	Slash	Low shade, >50% NPV.
7	Bare soil	Low shade, >80% soil; agriculture or construction areas.
	Roads	Low shade, >80% soil; unpaved.

Sabol et al. (2002) used simple linear mixture model to identify states of re-growth in replanted clear cuts in Douglass-fir/western hemlock forest in the Gifford Pinchot National Forest, Southern Washington, USA. The gain and offsets were used to calibrate TM images and sun-canopy-sensor correction was used to remove shade due to topography. The four reference endmembers of green vegetation, non-photosynthesis vegetation, soil, and shade were collected based on laboratory measurement. Those four endmembers were input to LSMA model to produced fraction images. The fraction images were compared with United State Forest Service (USFS) database to show relationship of fraction images and USFS stand structure classes. Canopy attributes measured by SMA was similar to the USFS database. So, SMA could be useful for map structural stages of forest.

Lu et al. (2003) classified the secondary succession stage forest of the Rondonia region of Brazilian Amazon using LSMA. Three endmembers of shade, soil, and green vegetation were identified from scatter-plot of TM band 3 and band 4 and scatter-plot of band 4 and band 5. Those three endmembers fraction images were acquired through LSMA model. Four classification methods were applied to different sets of images - 1) MLC on original Landsat5 TM images, 2) MLC on green vegetation and shade fraction images, 3) thresholding definitions based on green vegetation and shade fractions, and 4) thresholding definitions based on shade-to-green vegetation ratio images were used to classify fraction images. The thresholding definition is a range of appropriate fraction associated with each land-use class. It can be defined by use of statistics (minimum, maximum, mean, and standard deviation) of selected area of interest (AOI) of each class. Results indicated that thresholding definitions based on shade-to-green vegetation ratio images provided highest overall

classification accuracy (78.22%) and MLC on original Landsat5 TM images provided lowest overall classification accuracy (70.79%). For MLC on green vegetation and shade fraction images and thresholding definitions based on green vegetation and shade fractions provided quite similar overall accuracy (77.23% / 76.73%)

Matthias and Martin (2003) used the linear unmixing model and NDVI to map a degree of impervious surface in Cologne-Born, Germany. Vegetation abundance data can be used as indicator to identify degree of impervious surface because less vegetation shows more impervious surface. MNF transformation was applied to ASTER data to produce MNF images. First three MNF images with 52.5%, 33.3%, and 6.2% of variability were used to select endmember. The three endmembers of bright built up area, bright green vegetation, and dark water/shadow were selected from scatter-plot of MNF images and fraction images were produced by linear unmixing model. The ASTER data were also converted to Normalized Difference Vegetation Index (NDVI) image to define vegetation abundance and compare with vegetation fraction from linear unmixing model. Figure 2.1 shows correlation of green vegetation, NDVI, and built up fraction with the degree of impervious surface from field check. Green vegetation fraction and NDVI show good negative relationship with impervious surface. Thus, Green vegetation fraction and NDVI were transformed into spatial distribution of imperviousness. The imperviousness distribution shows good results compared with field check.

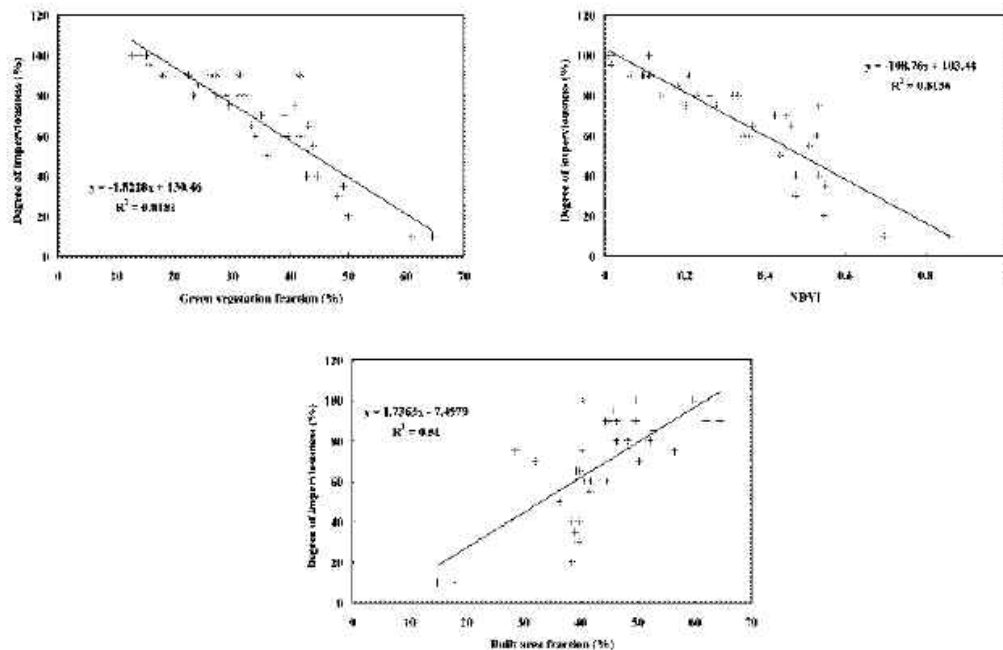


Figure 2.1 Relationship of green vegetation fraction, NDVI, and built up fraction with the field measurements of impervious surface. (Matthias and Martin, 2003)

Wu and Murray (2003) used LSMA model to estimate impervious surface distribution in metropolitan area of Columbus, Ohio, USA by use of Landsat ETM⁺. The V-I-S model was developed based on the vegetation, soil, high albedo, and low albedo spectral reflectance. Four endmembers of high albedo (e.g. concrete, clouds, and sand), low albedo (e.g. water and asphalt), vegetation (e.g. grass and trees), and soil were identified from scatter-plot of MNF transformation. LSMA was run with those four endmembers to get the vegetation, soil, high albedo, and low albedo fraction images. The impervious surface fraction image was developed using high and low albedo fraction images through the relationship in equation 2.1. Then, the pixel was considered as a combination of three endmembers as vegetation, soil, and impervious surface. Root mean square error (RMSE) was used to assess the accuracy

of impervious surface distribution corporate with the Digital Orthophoto Quarter Quadrangle (DOQQ) images. Result shows 10.6% of overall RMSE.

$$R_{imp,b} = f_{low} R_{low,b} + f_{high} R_{high,b} + e_b \quad (2.1)$$

Where $R_{imp,b}$ is the reflectance spectral of impervious surface for band b.

f_{low} and f_{high} are the fraction of low albedo and high albedo.

$R_{low,b}$ and $R_{high,b}$ are the reflectance spectral of low albedo and high albedo for band b.

Lu and Weng (2004) developed Lu and Weng conceptual model based on SMA method to analyze characteristics of urban LULC pattern of Indianapolis city, USA. The MNF transformation was used to transform Landsat ETM⁺ images into MNF images. The five endmembers of shade, green vegetation, impervious surface, dark soil, and dry soil were selected from scatter-plot of the first three MNF images. Four different combinations of three or four endmembers were tested to find the best quality of fraction images as: 1) four endmembers of shade, green vegetation, impervious surface, and dark soil, 2) three endmembers of shade, green vegetation, and impervious surface, 3) three endmembers of shade, green vegetation, and dry soil, and 4) three endmembers of shade, green vegetation and dark soil. Each component was input to SMA model to create a set of fraction images. The hybrid procedure that combined MLC with decision tree algorithm was used to develop conceptual model (see one of examples in Figure 2.2). The conceptual model defined ten land-use types in terms of proportions of green vegetation, shade, soil/impervious surface. Those four combinations were used to develop different conceptual models. Results indicated that three endmembers of shade, green vegetation, and dry soil showed best quality of both

urban and agricultural area. The combination of shade, green vegetation, and impervious surface endmembers provided satisfied results in urban area but poor in agricultural area. In contrast, with shade, green vegetation, and dark soil combination it showed satisfied results in agricultural area but poor in urban area. For four endmembers, a result was poor in both agricultural and urban areas.

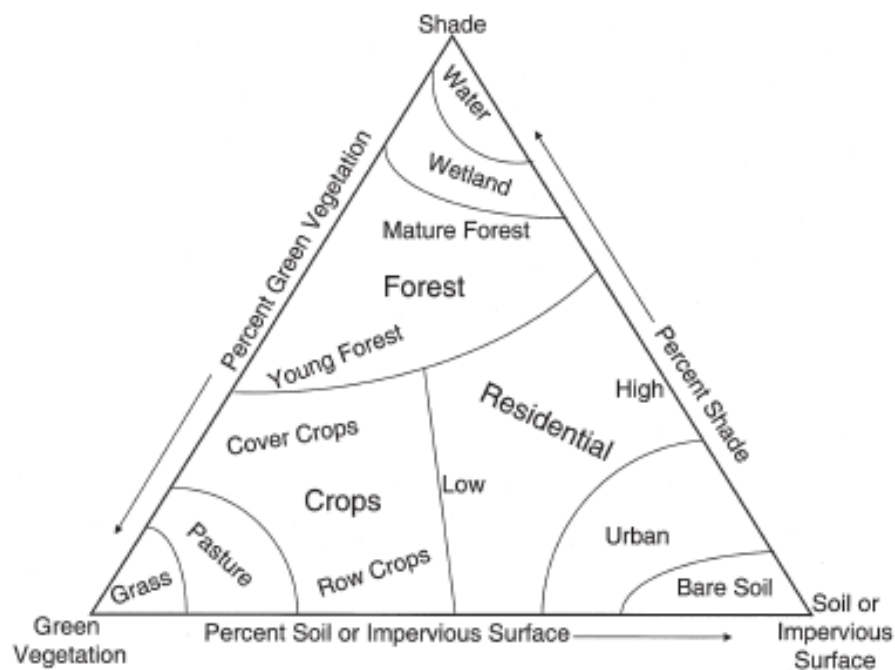


Figure 2.2 A Lu-Weng conceptual model (Lu and Weng, 2004)

Kardi (2007) applied linear spectral unmixing to Landsat images to characterize a pattern of urban areas in South-central Estonia (Tartu), Estonia. The three time spans of Landsat TM/ETM+ acquired on 1988, 1995, and 2001 were used. The vegetation, impervious surface, soil, and shade endmembers were extracted from a scatter-plot of PCA images and those four endmembers signatures were used to produce fraction images of vegetation, impervious surface, soil, and shade. Accuracy of interpreted urban area from fraction images was evaluated the one of the year 1995

by comparing with the Estonian basic map at the scale of 1:10,000. Overall error was 9%. For vegetation and soil fractions, they were overestimated by 6%, and impervious surface was underestimated by 15%. Temporal changes of vegetation, soil, and shade fractions were detected using these images too.

CHAPTER III

RESEARCH PROCEDURE

In this chapter, the details of research procedure are described. It includes a flow chart of research procedure, data and instrument used, and data analysis. The data analysis consists of LSMA for fraction images generation, MLC and EMC for urban LULC classification, and error matrix for accuracy assessment.

3.1 Research Methodology

The study aims at using MLC and EC to classify urban LULC Amphoe Muang Nakhon Ratchasima through TM images and fraction images derived from SMA. The classification accuracy resulting from using fraction images is expected to be higher than using the original Landsat TM classification.

The flow chart of research procedure is shown in Figure 3.1. The methodology can be divided into five major parts: 1) to prepare satellite images and aerial photographs, 2) to generate fraction images using LSMA technique (see flow chart in Figure 3.2), 3) to classify fraction images using EMC, 4) to classify LULC of the study area using MLC on Landsat5 TM image and on fraction images, and 5) to compare accuracies of the classifications.

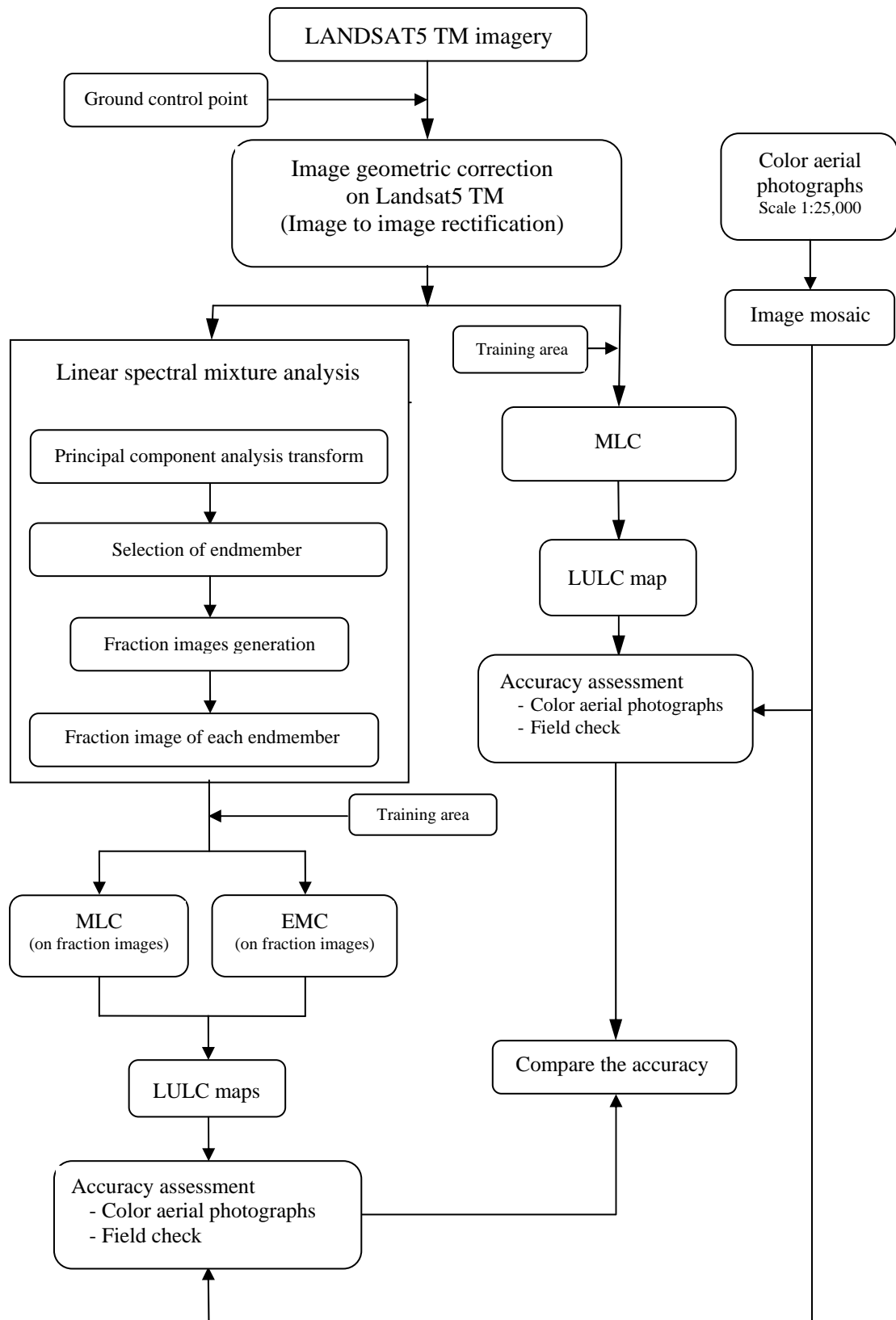


Figure 3.1 Flow chart of the research procedure

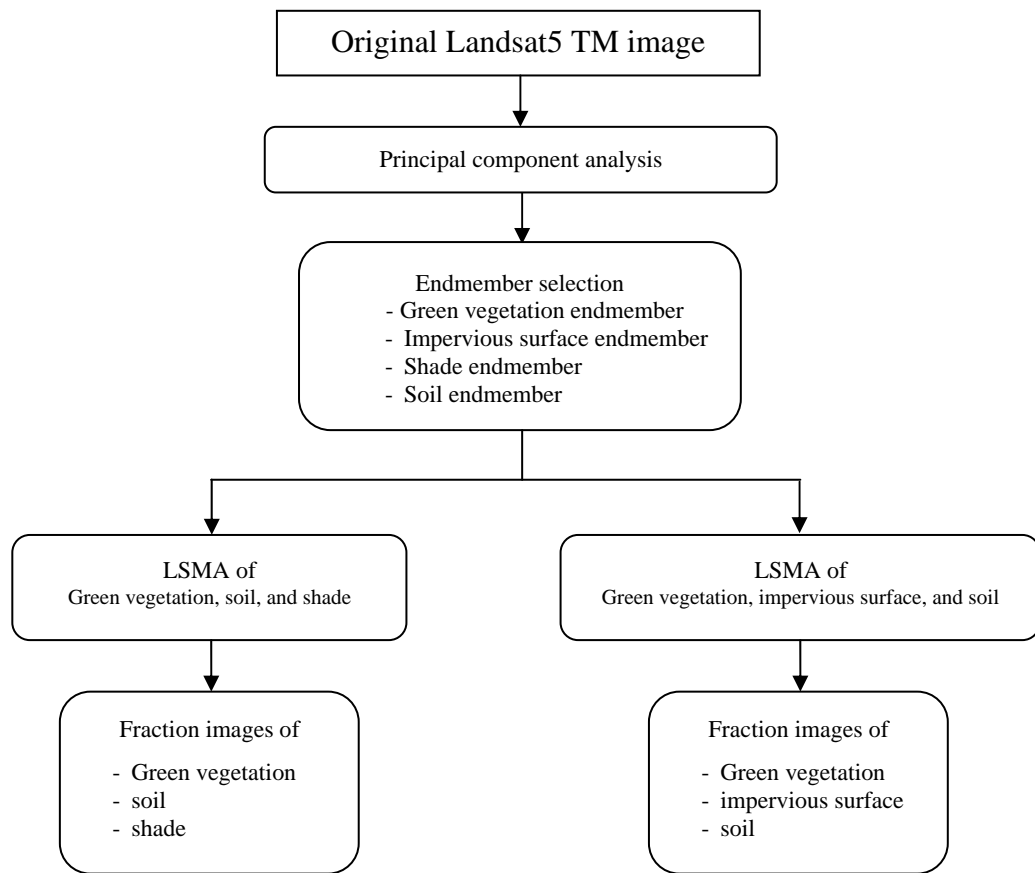


Figure 3.2 Flow chart of LSMA method

In the part of preparing satellite images, two types of images used are Landsat5 TM images and color aerial photographs covering Amphoe Muang Nakhon Ratchasima. The color aerial photographs of Ministry of Agriculture and Cooperatives with an existing coordinate system; UTM WGS 1984 zone 48 north, are mosaicked and used as reference images for image to image rectification. Landsat5 TM data of path 128 and row 50 with clear sky condition are cut and rectified based on the color aerial photographs with scale of 1:25,000 using ERDAS IMAGINE software. The color aerial photographs are also used as reference for selecting training areas and accuracy assessment.

The LSMA technique consists of three steps: 1) principal component transformation to reduce data redundancy and help user to select precisely pure reflectance signature of component, 2) endmember selection to select pure reflectance signatures of certain components in the scatter-plot of principal component images (pure reflectance signature will locate in a vertices of data cluster) and 3) LSMA which results in fraction images of each LULC component. A fraction image of a component is a percentage of the component containing in a pixel. Number of fraction images depends on the number of pure reflectance signatures input to the LSMA equation.

EMC is a classification method used to classify fraction images based on threshold range or classification limit of composition acquired from ternary plot. These fraction images result from LSMA i.e. fraction images of V-I-S and V-S-Sh composition.

MLC is a classification method using decision rule based on a probability to assign a pixel to corresponding class. The MLC is used to classify LULC of the study area on both original Landsat5 TM images and fraction images result from LSMA (V-I-S and V-S-Sh). The same set of training areas is used for both. Reference data within training areas are collected by use of field survey and those color aerial photographs.

Accuracy of LULC maps achieved from both EMC and MLC on fraction images and TM images are estimated using error matrix and Kappa statistics. The errors are calculated by comparing LULC maps with reference data from color aerial photographs and field survey. The classification accuracy from both techniques is compared to each other.

3.2 Data and Instrumentation

1. ERDAS IMAGINE9.0 Software, ENVI4.2 software, and ArcMap software package.
2. Cspace1.01 software, use to set up a classification condition from ternary plot.
3. Global positioning system (GPS)
4. Landsat5 TM imagery path-row 128-50 of Muang Nakhon Ratchasima area acquired in 2005
5. Color aerial photographs of Ministry of Agriculture and Cooperatives with scale of 1:25,000 acquired in 2002.
6. Field data used as reference in accuracy assessment.

3.3 Data Analysis

The data analysis for this research consists of five steps (Table 3.2) which are LSMA to achieve fraction images, EMC to classify urban LULC from fraction images, MLC to classify urban LULC from fraction images and the original Landsat5 TM images, accuracy assessment using Error matrix and Kappa statistics to evaluate accuracy of LULC classifications, and finally accuracy comparison of LULC classifications from both fraction images and the original Landsat5 TM images.

Table 3.1 Summarized methods used for data analysis.

Method	Data	Result
LSMA	Landsat5 TM images	Fraction images of endmember
EMC	Fraction images of V-I-S and V-S-Sh combination	LULC map from fraction images
MLC	Landsat5 TM images	LULC map from Landsat5 TM images
	Fraction images of V-I-S and V-S-Sh combination	LULC map from fraction images
Accuracy assessment (Error matrix and Kappa statistics)	LULC map from Landsat5 TM images	% accuracy of LULC classes from Landsat5 TM images
	LULC map from fraction images	% accuracy of LULC classes from fraction images
Classification accuracy comparison	% accuracy of LULC classes from Landsat5 TM images	Method which results the best accuracy
	% accuracy of LULC classes from fraction images	

3.3.1 Linear spectral mixture analysis

From linear spectral mixture equation (see appendix A), input data is DN_s from original Landsat5 TM images and results of this equation are fraction images of endmembers. Before running the equation, a unique spectral reflectance of a pure ground component (endmember, DN_{ik}) has to be selected. In this research, the endmembers will select from the cluster data in scatter-plot of principal component images achieved from Landsat5 TM data. Number of endmembers can be varied from 3 to 6 because of the limitation of number of TM bands. For this research, it is varied as 3 and 4 endmembers of green vegetation, impervious surface, soil, and shade. To

find a best quality of fraction images, the two different combinations of endmember are test, 1) combination of V-I-S and 2) combination of V-S-Sh.

3.3.2 LULC classification

The LULC class will classify in to eight classes as CBD, residential, grass field/bare soil, horticultural area, shrub, paddy field, forest, and water for the original TM images, V-S-Sh fraction images and seven classes exclude water for V-I-S fraction images. Reference data of each training area are selected based on field survey and color aerial photographs. LULC classifications consist of two methods as EMC and MLC.

- EMC is a classification method set up to perform: 1) to define the composition limits of three components (from fraction images) of each LULC class in the training area by plotting in ternary diagram of CSpace1.01 software. The plotted point data corresponding to each LULC class will be grouped together and the different classes tend to be separated from each other, 2) to classify each pixel of fraction image to LULC class based on composition limits of three components by use of ERDAS Modeler function, 3) to combine LULC map of each class to be LULC map of the study area which contains all classes using ERDAS Knowledge classification function. EMC is used to classify fraction images of V-I-S and V-S-Sh combinations.

- MLC is conventional classification method used to classify original Landsat TM images, fraction images of V-I-S and V-S-Sh combinations.

3.3.3 Accuracy assessment (Error matrix)

Accuracies of five classification maps based on different sources and techniques i.e. MLC on original Landsat5 TM, MLC on V-I-S model, MLC on V-S-Sh model, EMC of V-I-S model and EMC of V-S-Sh model are assessed using Error matrix to find overall accuracy, producer's accuracy (PA), user's accuracy (UA) and kappa statistics with the reference data from field survey and color aerial photographs from Ministry of Agriculture and Cooperatives covering the study area.

3.3.4 Comparison of LULC classification accuracies

Four different types of LULC classification accuracies - overall accuracy, PA, UA and kappa statistics from different types of images and techniques mentioned above are compared. The overall accuracy computes by dividing the total number of correct pixels by the total number of pixels. The kappa statistics of all classes can be computed using equation 3.1 (Jensen, 2005).

$$\hat{K} = \frac{N \sum_{i=1}^k X_{ii} - \sum_{i=1}^k (X_{ii} \times X_{+i})}{N^2 - \sum_{i=1}^k (X_{i+} \times X_{+i})} \quad (3.1)$$

Where \hat{K} is Overall Kappa statistic.

X_{ii} is number of observations correctly classified for a particular category.

X_{i+} and X_{+i} are the marginal totals for row i and column i associated with the category.

N is the total number of observations in the entire error matrix.

CHAPTER IV

DATA AND DATA MANIPULATIONS

The Landsat5 TM data used in this study supported by Geo-Informatics and Space Technology Development Agency (Public Organization) or GISTDA were acquired on 6 March 2005 (Systematic Geo-correction product of path 128 rows 50) in dry season with clear sky condition as shown in Figure 4.1

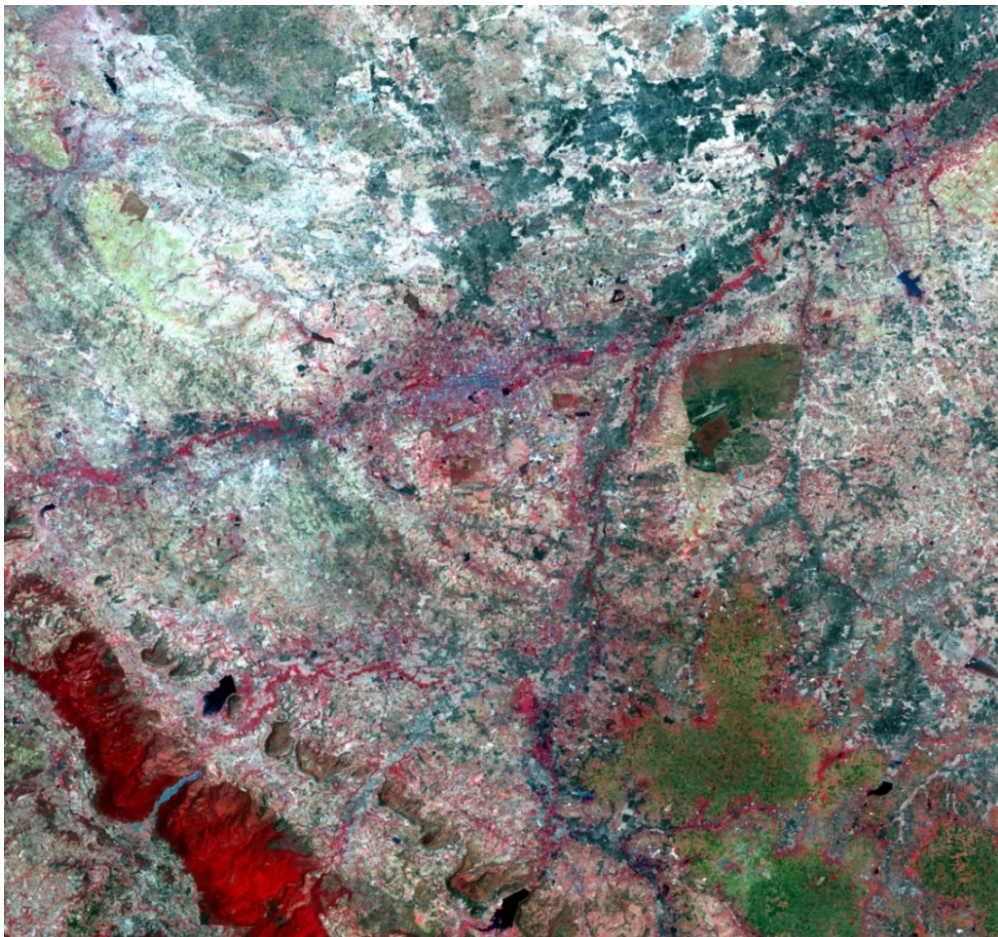


Figure 4.1 Landsat5 TM images, displayed in false colors composite with RGB: 432 covering Nakhon Ratchasima province.

The color aerial photographs acquired on 2002 from Ministry of Agriculture and Cooperatives scale 1:25,000 with an existing coordinate system of UTM WGS 1984 zone 48 north was used as reference for image to image rectification with Landsat5 TM. The twenty one scenes of aerial photographs cover Amphoe Muang Nakhon Ratchasima urban area were previously mosaiced and resampled to 1m resolution before using as reference (Figure 4.2).

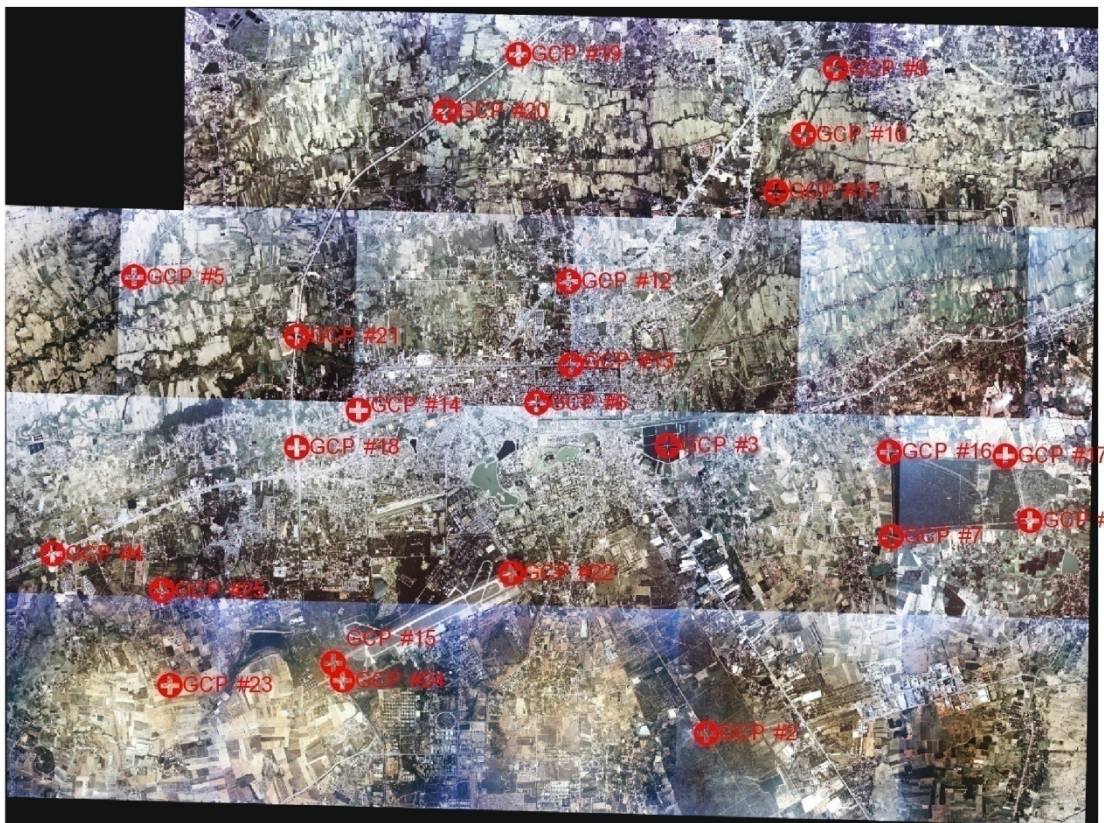


Figure 4.2 The 21 mosaic scenes of aerial photographs were used as reference image for Landsat5 TM rectification.

Landsat TM images were rectified using second order of polynomial equation from ERDAS IMAGINE software package. The twenty five control points collected from color aerial photographs were used to match the same location in TM images and rectified with resampling to 25 x 25 m pixel size by the nearest neighborhood

algorithm. The RMSE obtain from the rectification process is 0.665 pixel or 16.63 m ($25 \times 0.665 = 16.3$). Table 4.1 and 4.2 show statistics of the model and transformation parameters for the rectification.

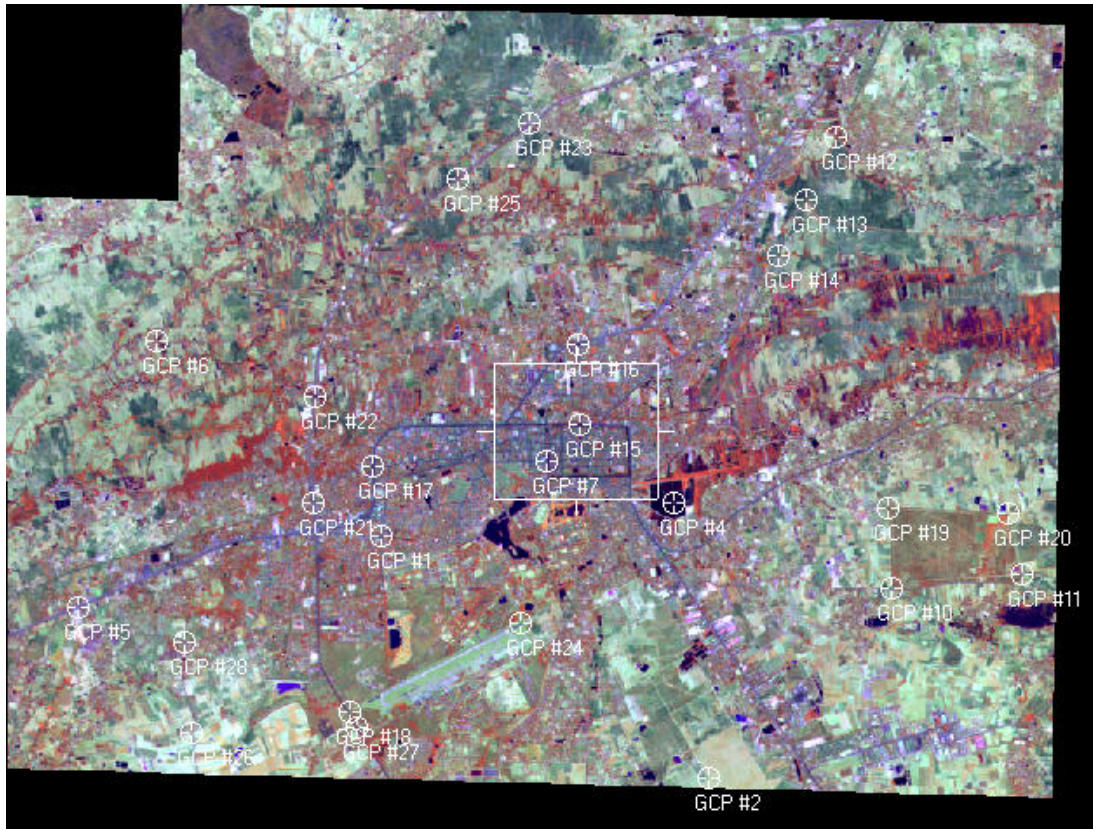
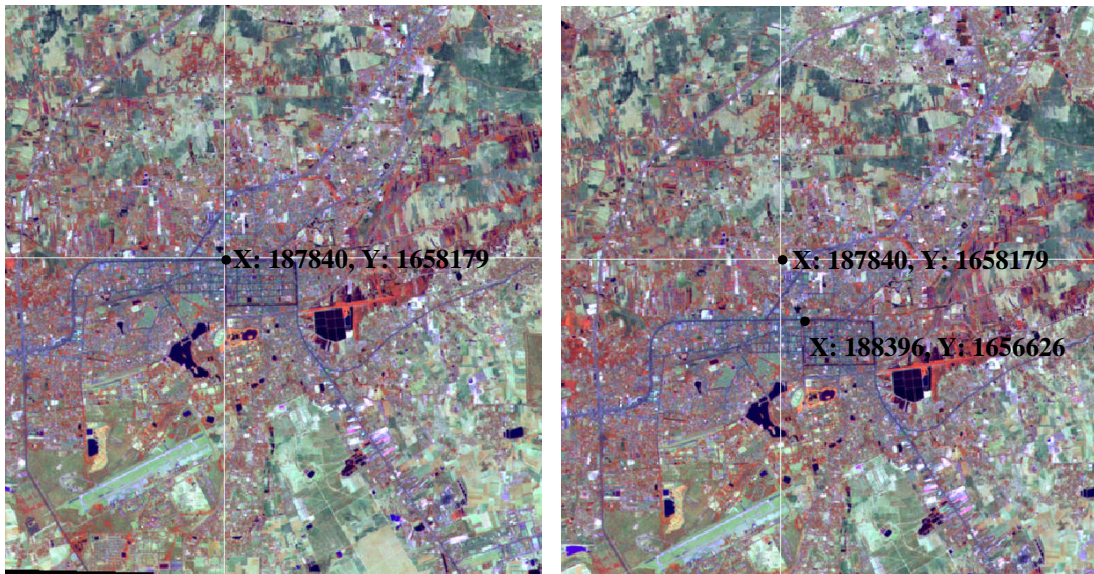


Figure 4.3 Landsat5 TM covering Muang Nakhon Ratchasima municipal with the twenty five reference points from color aerial photographs, displayed in false color composite with RGB: 453.

The white box shows in the Figure 4.3 is the study area which covers urban area of Amphoe Muang Nakhon Ratchasima. Figure 4.4 illustrates the shift of rectified TM images from the original image. The rectified image was shifted to the north about 1,553 m and to the west about 556 m.



a) original image

b) rectified image

Figure 4.4 Comparison of the original image (a) and the rectified image (b) of TM5 covering the study area, displayed in false colors with RGB: 453.

Table 4.1 The transformation parameters of the rectification.

Row	X'	Y'
const	-888822	301773
X	0.743727	-0.429048
Y	1.10059	0.684393
X^2	-1.63314e-8	-9.94026e-8
xy	1.58996e-7	2.82633e-7
Y^2	-3.4057e-7	7.85969e-8

The transformation parameter for X' and Y' shows in equation 4.1 and 4.2

$$X' = -888822 + 0.743727X + 1.10059Y + 1.58996e^{-7}XY - 1.63314e^{-8}X^2 - 3.4057e^{-7}Y^2 \quad (4.1)$$

$$Y' = 301773 - 0.429048X + 0.684393Y + 2.82633e^{-7}XY - 9.94026e^{-8}X^2 + 7.85969e^{-8}Y^2 \quad (4.2)$$

Table 4.2 The statistical data of the 2nd order polynomial model for image rectification.

	X-residual (m.)	Y-residual (m.)	RMS error (m.)
Count	25.00	25.00	25.00
Total	0.00	0.00	415.69
Min	-28.96	-38.53	0.00
Max	25.87	22.54	30.63
Mean	0.00	0.00	16.63
Std. dev	14.62	14.05	8.57

CHAPTER V

LULC MAPS AND ACCURACY ASSESSMENTS

The chapter describes results of manipulation and analytical processes of the study, namely, training area selections, LULC classifications, and accuracy assessments. LULC classifications in this study were composed of two methods, MLC and EMC. The MLC was used to classify both original Landsat5 TM images and fraction images derived from LSMA technique. The EMC was used to classify only the fraction images of V-I-S and V-S-Sh combinations. The accuracy assessments were performed for results of all classifications and compared.

5.1 Training Area Selection

Training area selection is an important step of the classification. Training areas must be homogeneously and represent LULC classes. There are many ways to collect training data which include 1) collecting from field information (ground survey), 2) on screen selecting training data as polygons, and 3) on screen seeding of training data (Jensen, 2005). For this research, training areas were selected from ground survey and on screen based on reference images (aerial photographs). Most of training areas were selected on screen and only some were selected from ground survey when LULC was complicate.

The LULC of study area could be classified into eight classes as horticultural area, grass field/bare soil, forest, residential, CBD, shrub, paddy field, and water.

Figure 5.1 and 5.2 illustrate the training sites selected for classifications.



Figure 5.1 Training sites selection for the classifications.

5.2 Linear Spectral Mixture Analysis

LSMA is an approach to classify multispectral data in sub-pixel level. It shows relationship between mixed spectral reflectance of a pixel and fractions of ground component that contain in the pixel. LSMA involves two steps: 1) to find the unique spectral reflectance signature of a pure ground component or an endmember. The endmember is selected from scatter-plot of principal component values which results from the principal component transformation process. The pure reflectance signature will locate in the vertices of data cluster. 2) to extract the fraction area of each component in a pixel which has linear combinations of endmembers by running

LSMA equation. It results in a fraction image of each component/endmember. Each pixel of a fraction images contains an area percentage of the component in a pixel.

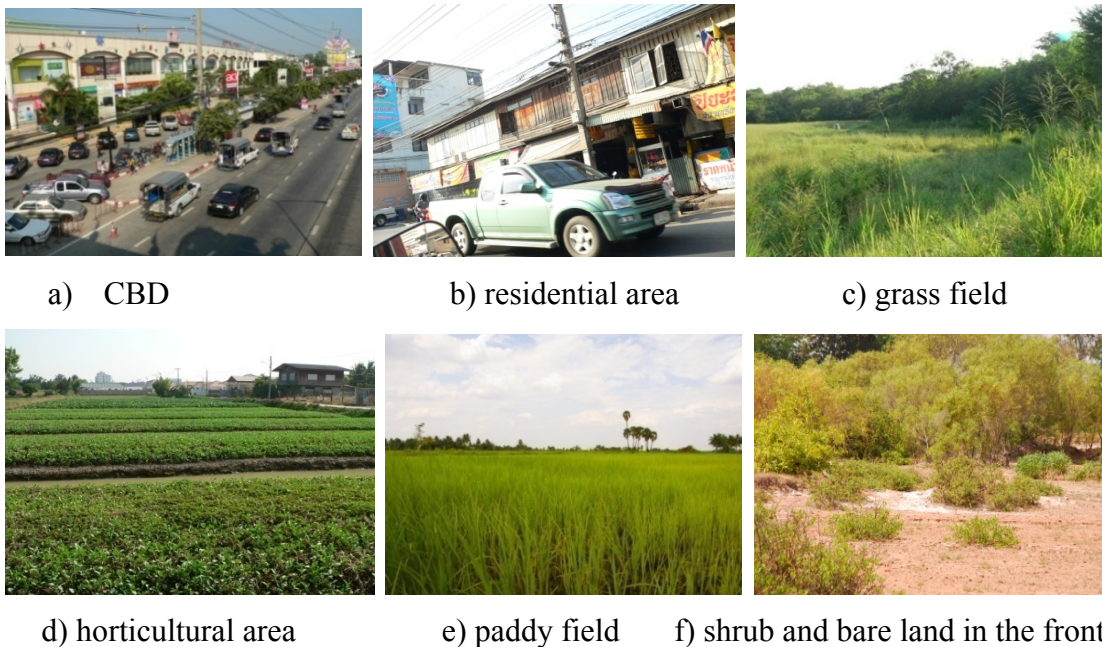


Figure 5.2 Photos showing CBD (a), residential area (b), grass field (c), horticultural area (d), paddy field (e), and shrub and bare land in the front (f) of Nakhon Ratchasima municipality.

5.2.1 Principal component transformation

The PCA was applied to transform 6 reflection bands of Landsat 5 TM data (excluding thermal band) to 6 principal component images. Only first 3 images (Figure 5.3) were chosen for LSMA because they have higher potential information. The higher potential image is indicated by its PCA eigenvalue. The higher eigenvalue shows higher variance in the image which means that the image has lower data redundancy.



a) PC1 of study area



b) PC2 of study area

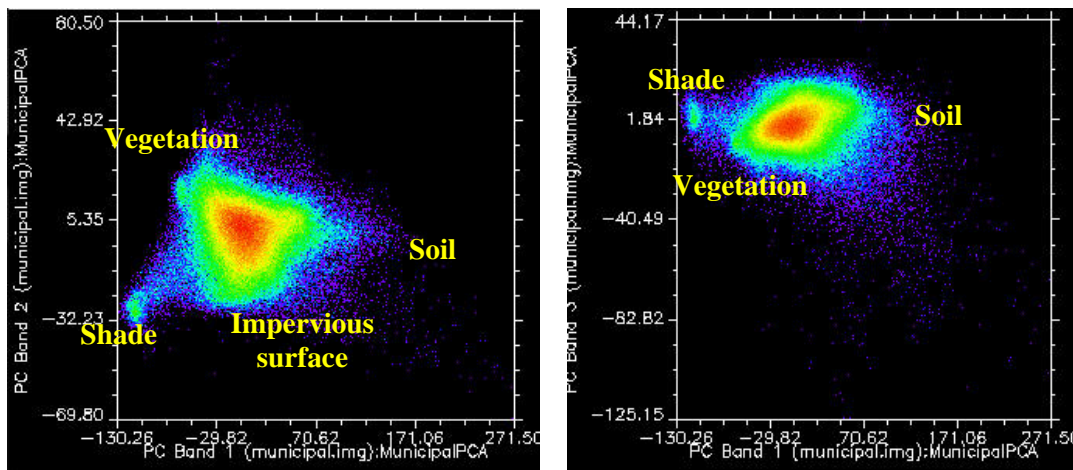


c) PC3 of study area

Figure 5.3 PC1, PC2, and PC3 images of study area.

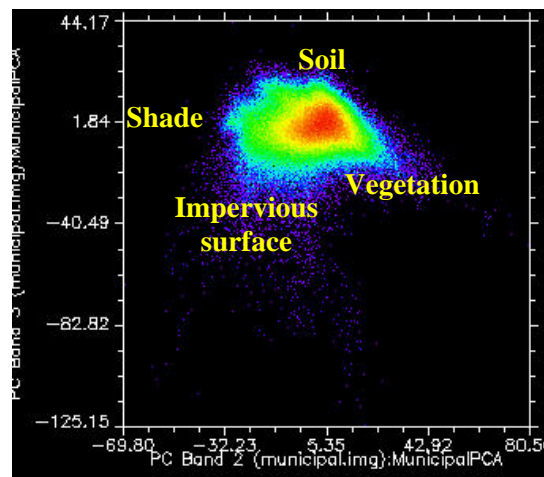
5.2.2 Endmember selection

According to the scatter-plots of those principle component values as shown in Figure 5.4, four endmembers of soil, green vegetation, shade, and impervious surface with unique spectral reflectance signatures were selected. The impervious surface comprises road, building roof, and airport runway. The unique signatures show narrow standard deviations. Spectral reflectance signature of the shade mostly matched to water body within the study area. Figure 5.4 shows the unique or pure signature pixel of the shade, soil, green vegetation, and impervious surface endmembers that were used as AOI (area of interest) in LSMA model.



a) Plot of PC1 and PC2

b) Plot of PC1 and PC3



c) Plot of PC2 and PC3

Figure 5.4 Scatter-plots of principal component images for municipal area: a) the plot of PC1 and PC2, b) the plot of PC1 and PC3, and c) the plot of PC2 and PC3

5.2.3 Fraction images generation

The unique signatures of those four endmembers of each TM band were separated into two different sets of combination: a) the three endmember combination of green vegetation, impervious surface, and soil (V-I-S), and b) the three endmember combination of green vegetation, soil, and shade (V-S-Sh). Each set was input to LSMA function of ENVI version 4.2 to attain a fraction image of each endmember.

Each pixel of certain image contains a value indicating proportionate area covered by a certain endmember.

5.2.3.1 The three endmember combination of green vegetation, impervious surface, and soil (V-I-S)

Results of LSMA for V-I-S were green vegetation, impervious surface, soil, and RMSE fraction images. First three images indicated proportion of certain endmembers in every pixel and RMSE indicated error of the model. The mean RMSE over images of V-I-S combination was 2.16. The bright area showed high percentage of certain fraction and darker gray showed lower percentage. For example, Figure 5.5b illustrating the impervious fraction image, road and structure area appears bright which mean that it had high percentage of impervious surface and low percentage of green vegetation and soil.

5.2.3.2 The three endmember combination of green vegetation, soil, and shade (V-S-Sh)

Results of LSMA for V-S-Sh were green vegetation, soil, shade, and RMSE fraction images. First three images indicated proportion of certain endmember in every pixel and RMSE indicated error of the model. The mean RMSE over images of V-S-Sh combination was 2.38. Figure 5.6 illustrates the fraction images of green vegetation, impervious surface, soil, and RMSE.

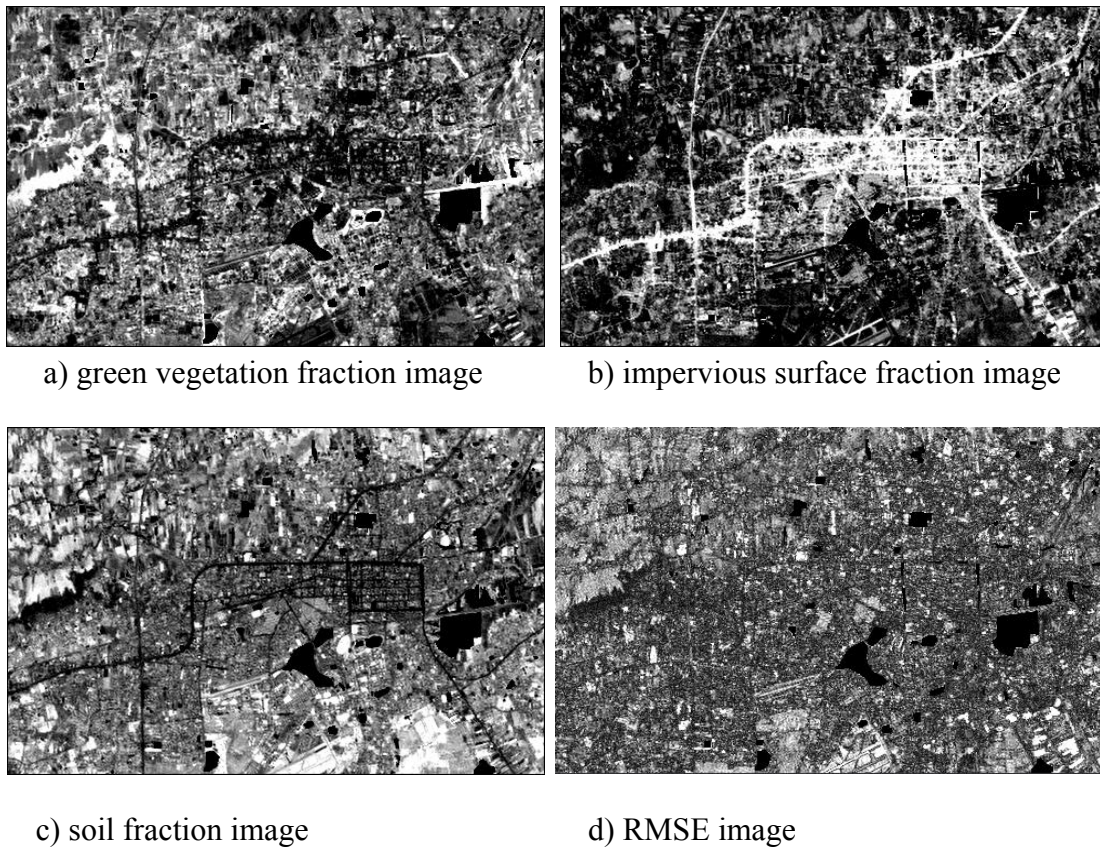


Figure 5.5 Shows the green vegetation, impervious surface, bare soil, and RMSE fraction images of the study area.

5.3 LULC Classifications

LULC classifications covered two main methods MLC and EMC. The MLC was used to classify original Landsat TM images, fraction images of V-I-S and V-S-Sh combinations. The EMC was used to classify fraction images of V-I-S and V-S-Sh combinations. The original Landsat TM images and fraction images of V-S-Sh combinations were classified into eight classes according to training areas selected. Fraction images of V-I-S were classified to seven classes excluding water. Accuracy assessments were performed for all classified LULC map using Error matrix and Kappa statistic.

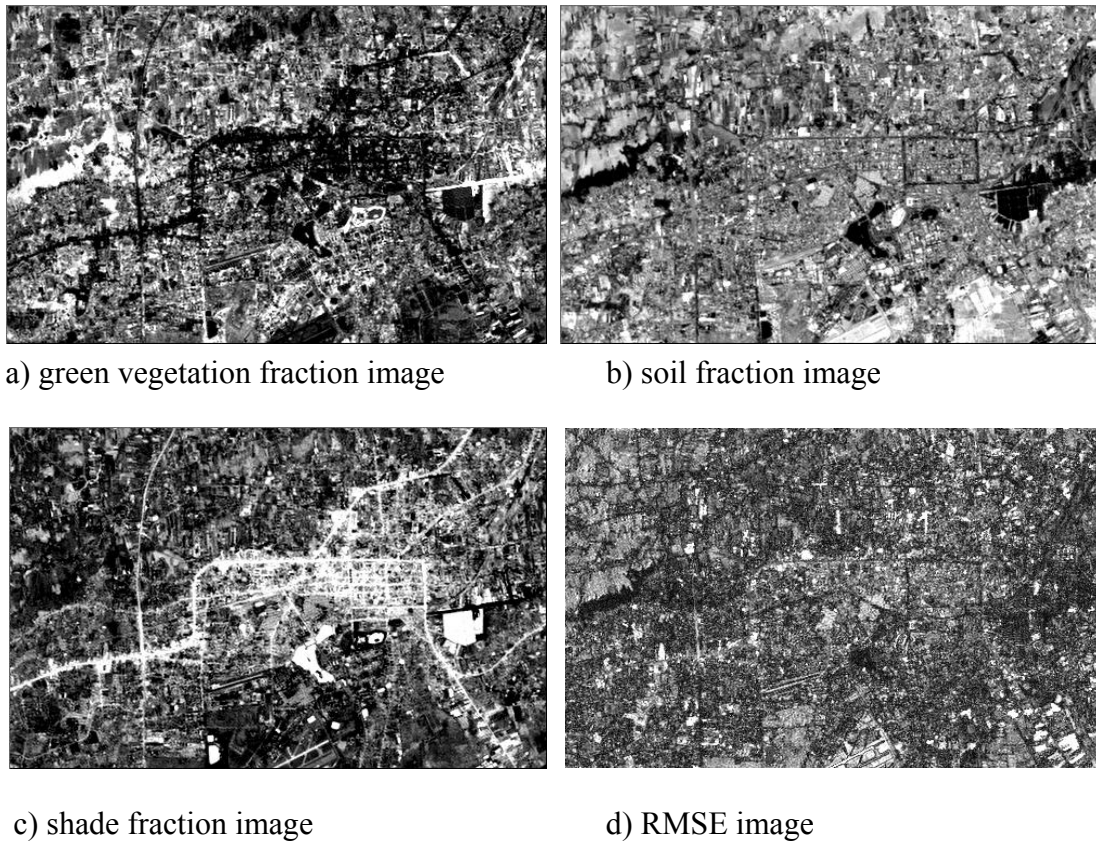


Figure 5.6 Shows the green vegetation, bare soil, shade, and RMSE fraction images of the study area.

5.3.1 Maximum likelihood classification of original Landsat5 TM images

The study area was classified into eight classes as forest, horticultural area, grass field/bare soil, residential area, CBD, shrub, and water. Training areas were collected more than 100 pixels for each class and MLC was performed. Results of the classification are presented in Figure 5.7 and Table 5.1. Residential covered largest area following by paddy field, shrub, CBD, grass field/bare soil horticultural area, forest, and water, respectively.

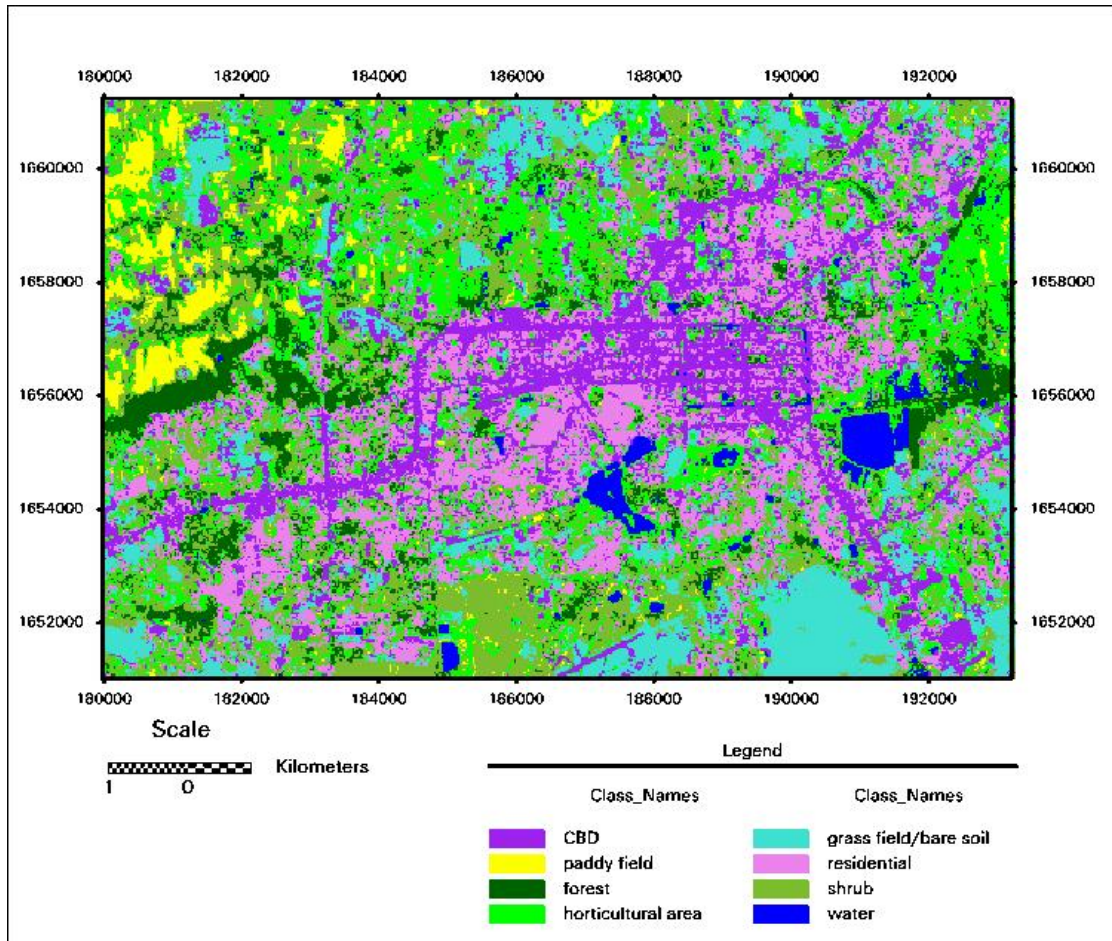


Figure 5.7 LULC map by MLC for original Landsat5 TM images.

Table 5.1 Pixel number and area of each class classified using MLC for original Landsat5 TM images.

LULC classes	Number of pixels classified	Class area (square meters)
CBD	25,079	15,674,375
Residential area	33,224	20,765,000
Grass field/bare soil	19,033	11,895,625
Shrub	28,409	17,755,625
Horticultural area	11,857	7,410,625
Forest	5,861	3,663,125
Paddy field	28,819	18,011,875
Water	3,462	2,163,750

5.3.2 Fraction images classifications

The fraction images of the V-I-S and V-S-Sh combinations were classified by two methods i.e. MLC and EMC. Training areas used for classification were the same set as used for MLC of the original Landsat5 TM images. For EMC, training areas were input to CSpace1.01 program to create ternary plot. The ternary plot was performed in triangular shape used to present relative percentage of three components summed up to 100%. Training point data were plotted in ternary diagram and plotted point data of each corresponding LULC class can be grouped together.

5.3.2.1 Maximum likelihood classification

The study area was classified into eight classes using fraction images of V-S-Sh combination and seven for V-I-S combination. Water was removed before running the classification of V-I-S fraction images because it was not related to green vegetation, impervious surface, and soil component. The same set of training areas was used for each LULC class and MLC was performed to each combination fraction images.

1) V-I-S fraction images

Results of classification are presented in Figure 5.8 and Table 5.2. Residential area was found covering largest area following by shrub, grass field/bare soil, horticultural area, CBD, forest, and paddy field, respectively.

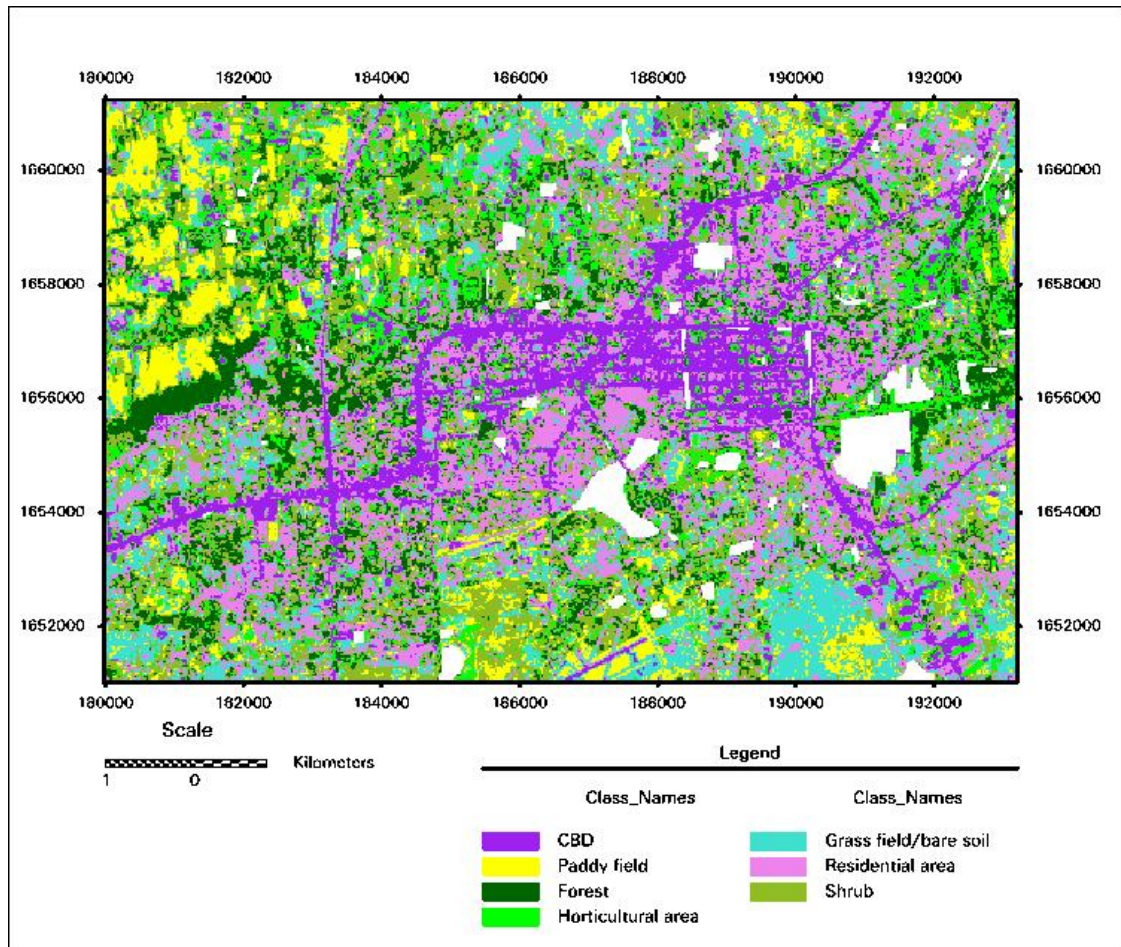


Figure 5.8 LULC map by MLC for V-I-S fraction images

Table 5.2 Number of pixels and area classified for each class of MLC for V-I-S fraction images.

LULC classes	Number of pixels classified	Class area (square meters)
CBD	18,036	11,272,500
Residential area	33,788	21,117,500
Grass field/bare soil	20,998	13,123,750
Shrub	27,573	17,233,125
Horticultural area	19,057	11,910,625
Forest	17,200	10,750,000
Paddy field	13,953	8,720,625

2) V-S-Sh fraction images

Results of classification are presented in Figure 5.9 and Table 5.3. Horticultural area was found covering largest area following by shrub, residential area, CBD, grass field/bare soil, forest, paddy field, and water, respectively.

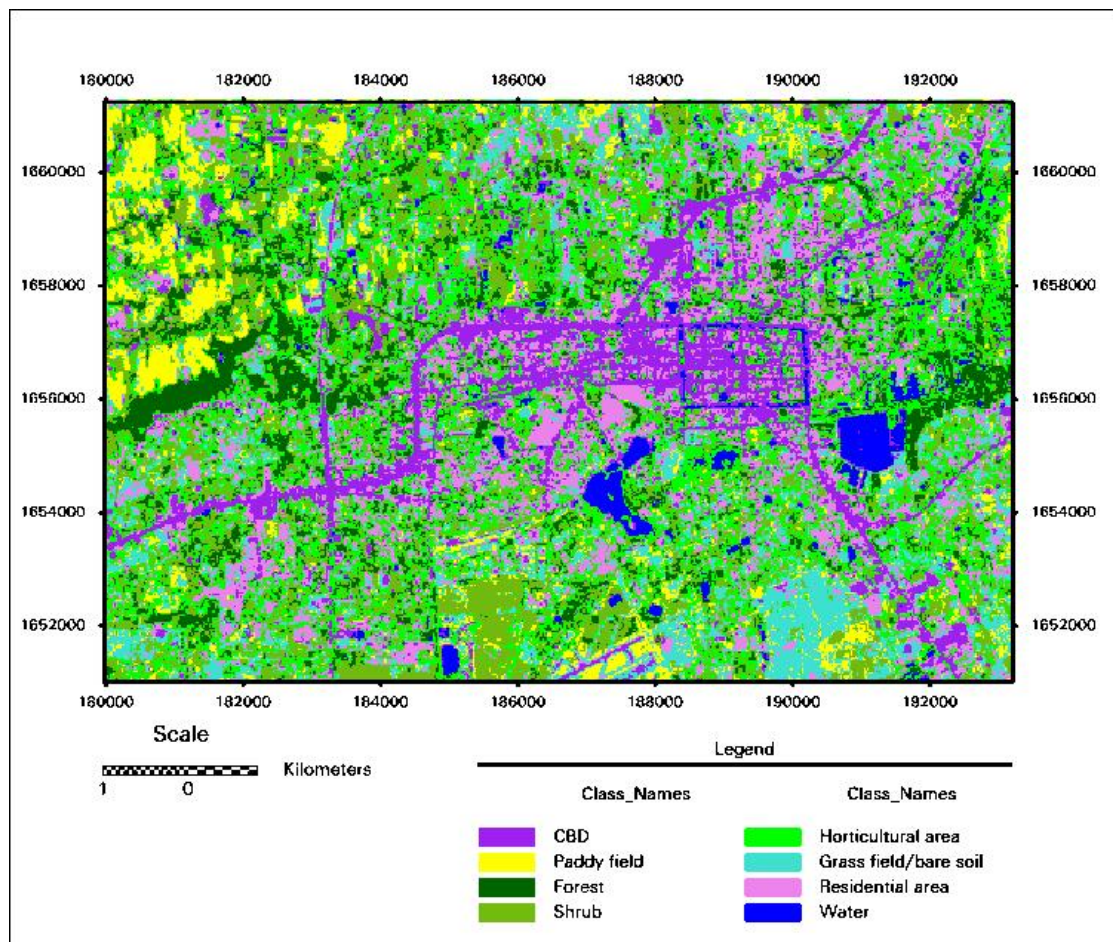


Figure 5.9 LULC map by MLC for V-S-Sh fraction images

Table 5.3 Number of pixels and area classified for each class of MLC for V-S-Sh fraction images.

LULC classes	Number of pixels in a class	Class area (square meters)
CBD	18,554	11,596,250
Residential area	23,380	14,612,500
Grass field/bare soil	17,419	10,886,875
Shrub	26,552	16,595,000
Horticultural area	40,244	25,152,500
Forest	14,542	9,088,750
Paddy field	11,310	7,068,750
Water	3,743	2,339,375

5.3.2.2 Endmember model classification

EMC was used to classify fraction images of V-I-S and V-S-Sh combinations. The classification consists of two steps: 1) to find the frame of classification limit for each LULC class plotting in ternary diagram. The same set of training data was input to CSpace1.01 software for ternary plot to define composition limits of three components for each LULC class. The plotted point data corresponding to each LULC class was grouped together and different classes tended to separate from each other. Therefore, a certain class tended to have its own frame/limits formed by certain proportions of the three components. 2) to classify each pixel of fraction images to a certain class based on proportions of three components through knowledge classification function.

1) V-I-S fraction images

LULC of the study area was classified in terms of proportions of green vegetation, impervious surface, and soil based on V-I-S combination from ternary plot showing in Figure 5.10. The frame of seven LULC classes of this EMC was input to modeler function of ERDAS IMAGINE software to create a LULC map for each class. After that seven separated LULC classes were combined together by use of knowledge classification function. Figure 5.11 and Table 5.5 show results of V-I-S combination classification map. Horticultural area covered largest area following by shrub, residential area, forest, CBD, paddy field, and grass field/bare soil, respectively.

Table 5.4 The definition of LULC types classified for V-I-S fraction images using endmember model.

LULC class	Definition
CBD	Less vegetation (usually less than 30%), more impervious surface (greater than 70%), and soil usually less than 30%.
Forest	Major vegetation (usually greater than 70%) and less impervious surface and soil.
Horticultural area	Moderate vegetation (47-70%), less impervious surface; and moderate soil.
Grass field/bare soil	Less vegetation and impervious surface (usually less than 30%), high soil (>70%).
Residential area	Moderate vegetation and soil, high impervious surface (usually greater than 60%).
Shrub	Moderate vegetation (40-60%); low impervious surface; and moderate soil (45-75%).
Paddy field	Low vegetation and impervious surface (usually less than 40%), high soil (greater than 70%).

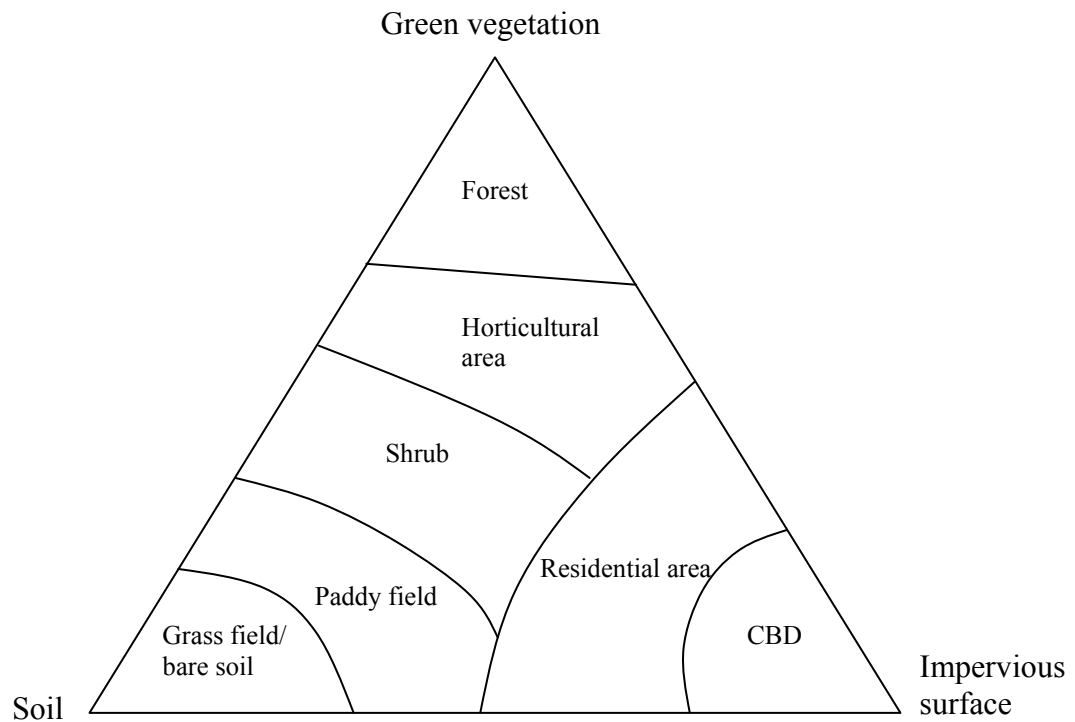


Figure 5.10 Ternary diagram of green vegetation, impervious surface, and soil (V-I-S) fractions of the study area.

Table 5.5 Number of pixels and area for each class of V-I-S fraction images using endmember model.

LULC classes	Number of pixels in a class	Class area (square meters)
CBD	13,214	8,258,750
Residential area	21,617	13,510,625
Grass field/bare soil	9,167	5,729,375
Shrub	27,758	17,348,750
Horticultural area	46,318	28,948,750
Forest	21,399	13,374,375
Paddy field	11,132	6,957,500

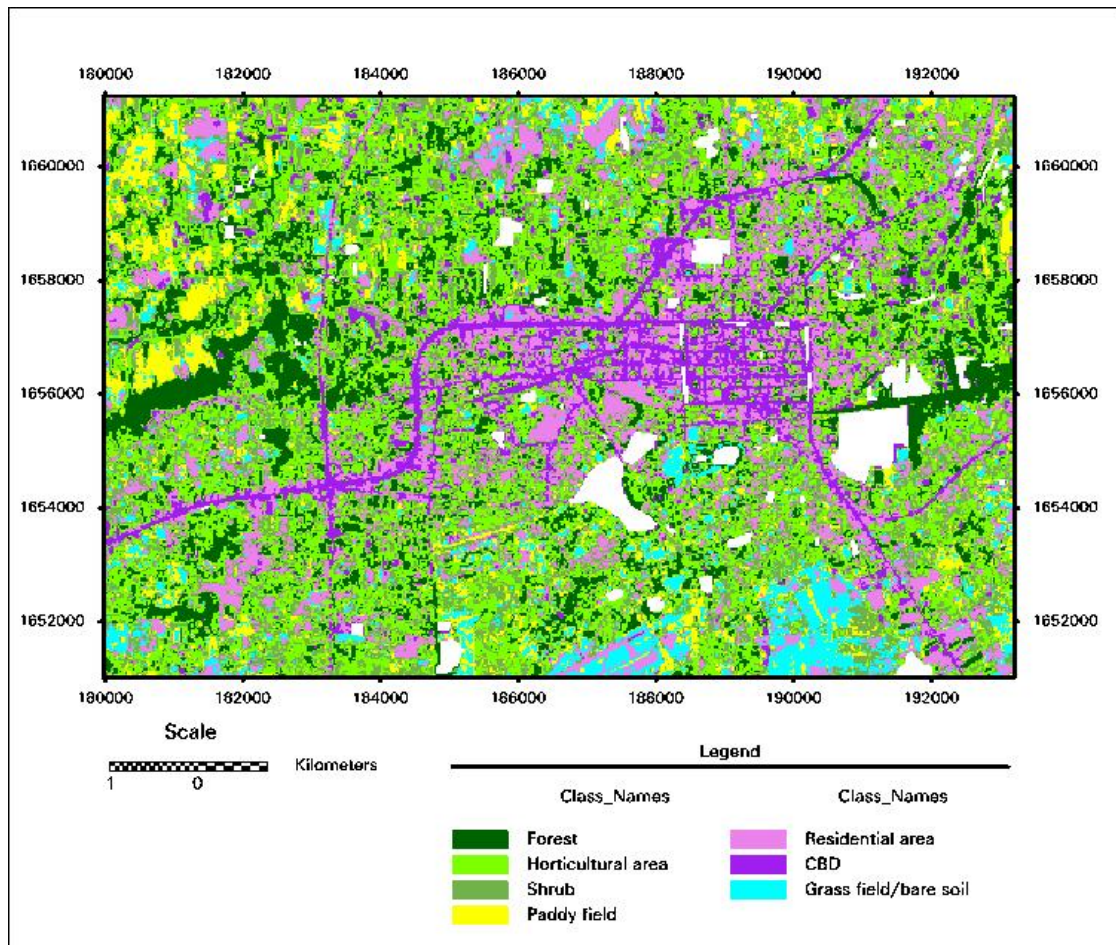


Figure 5.11 LULC map by EMC of V-I-S fraction images.

2) V-S-Sh fraction images

As same as classification made on V-I-S, the classification frame of eight LULC classes of V-S-Sh from ternary plot (Figure 5.12) was input to the modeler function to create a LULC classification map of the study area. After that separated eight LULC classes were combined together by use of knowledge classification function. Figure 5.13 and Table 5.7 were results of V-S-Sh classification map. Residential area has largest area following by paddy field, horticultural area, shrub, forest, grass field/bare soil, CBD, and water, respectively.

Table 5.6 The definition of LULC types classified for V-S-Sh fraction images.

LULC class	Definition
CBD	Less vegetation (usually less than 30%), less soil (usually less than 35%), and high shade (65-85%)
Forest	Major vegetation (usually greater than 70%), less soil (usually less than 30%), and moderate shade (< 45%).
Horticultural area	Moderate vegetation and soil (40-60%), and less shade (usually less than 40%)
Grass field/bare soil	Low vegetation and shade (usually less than 30%), high soil (greater than 70%).
Residential area	Moderate vegetation (usually less than 45%), moderate soil and shade (40-60%).
Shrub	Moderate vegetation (30-45%), high soil (40-65%), and low shade (usually less than 35%).
Paddy field	Less vegetation (30-40%), high soil (65-75%), and less shade (usually less than 40%).
Water	Major shade (usually greater than 80%), soil and vegetation were not detectable (<5%).

Table 5.7 Number of pixels and area for each class of V-S-Sh fraction images using endmember model.

LULC classes	Number of pixels classified	Class area (square meters)	Class area (square kilometers)
CBD	12,257	7,660,625	7.66
Residential area	31,822	19,888,750	19.89
Grass field/bare soil	17,986	11,241,250	11.24
Shrub	20,954	13,096,250	13.10
Horticultural area	22,627	14,141,875	14.14
Forest	20,722	12,951,250	12.95
Paddy field	27,167	16,979,375	16.98
Water	2,209	1,380,625	1.38

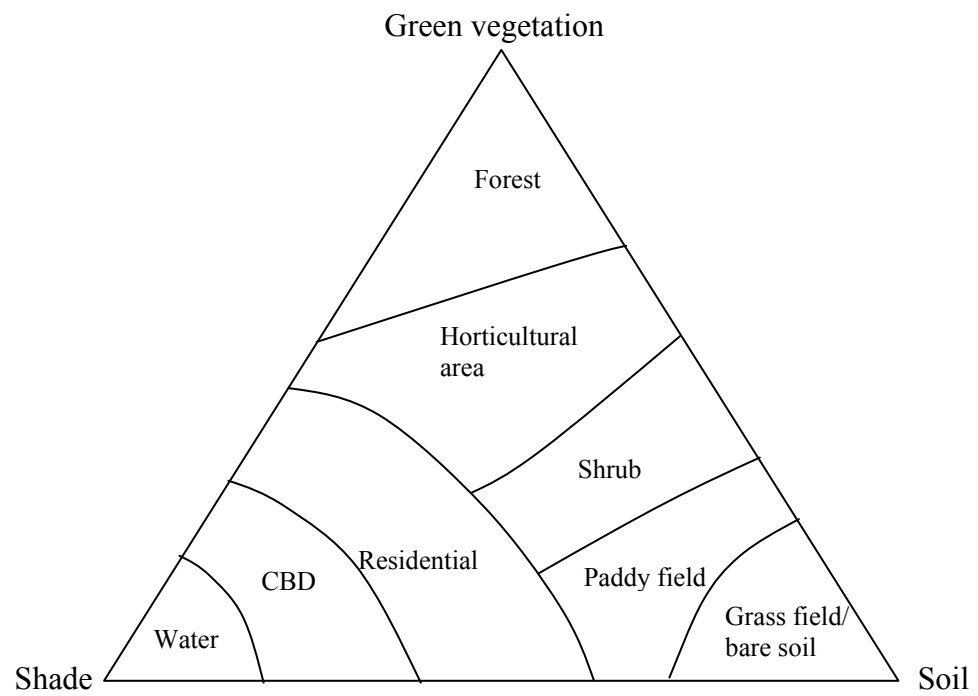


Figure 5.12 Ternary diagram of green vegetation, soil, and shade fractions (V-S-Sh) of the study area.

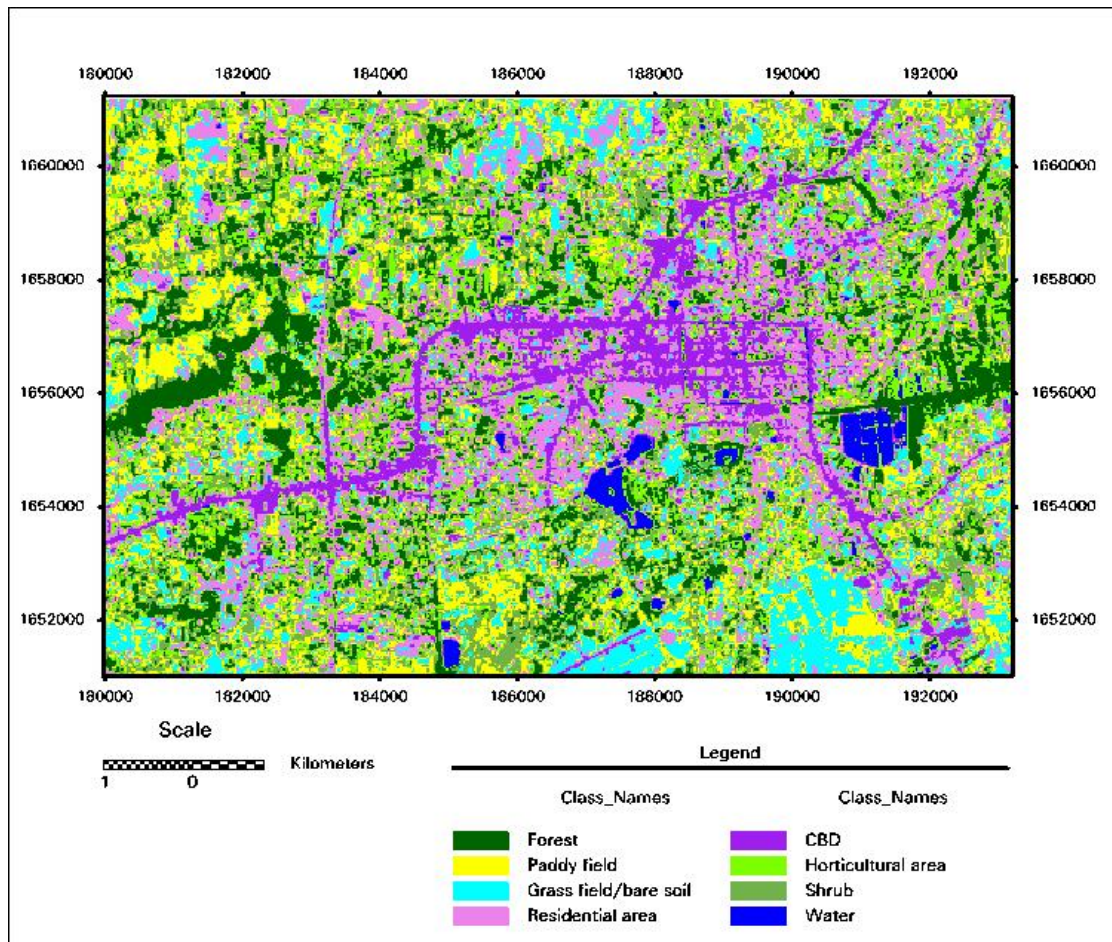


Figure 5.13 LULC map by EMC of V-S-Sh fraction images

5.4 Accuracy Assessments

Accuracies of five LULC maps based on different techniques were assessed using error matrix to find out the overall, producer's, and user's accuracies including overall Kappa statistic with reference data from color aerial photographs and field survey.

The number of samples used for error matrix was calculated based on multinomial distribution function which is suitable for a thematic map with multiple classes. The calculation of the number of samples for each class is as the following (Jensen, 2005).

$$N = \frac{B\Pi_i(1-\Pi_i)}{b_i^2} \quad (5.1)$$

Where Π_i is the proportion of a population in the i^{th} class, which has proportion closest to 50%, out of k classes.

b_i is the desired precision for this class

B is the upper $(\alpha / k) * 100$ th percentile of chi square distribution with 1 degree of freedom

k is the number of classes

For this research, the number of samples was calculated at a level of confidence = 85%, so $\alpha = 0.15$ and a precision $b_i = 0.05$, the number of classes (k) = 8 for original Landsat TM and fraction images of V-S-Sh combination and = 7 for fraction images of V-I-S combination. The total number of samples for all classification methods, which were used for accuracy determinations, were calculated based on equation 5.1 and shown in Table 5.8

B for seven and eight LULC classes calculated by

- B for seven classes: $1 - (\alpha / k) = 1 - (0.15 / 7) = 0.979$

With 1 degree of freedom, chi square $\chi_{0.979}^2 = 5.454$

- B for eight classes: $1 - (\alpha / k) = 1 - (0.15 / 8) = 0.981$

With 1 degree of freedom, chi square $\chi_{0.981}^2 = 5.668$

Table 5.8 Total number of samples and number of samples per class used for accuracy determinations.

Classification method	Proportion of area of the class closest to 50% out of the total area	$\frac{B\Pi_i(1-\Pi_i)}{b_i^2}$	Total number of samples/ number of sample per class
MLC of original Landsat5 TM images	$\frac{33224}{155744} = 0.213$	$\frac{5.668 \times 0.213 \times (1-0.213)}{(0.05)^2}$ = 380.07	384/48
MLC of V-I-S fraction images	$\frac{33788}{150605} = 0.224$	$\frac{5.454 \times 0.224 \times (1-0.224)}{(0.05)^2}$ = 379.1	385/55
MLC of V-S-Sh fraction images	$\frac{40244}{155744} = 0.258$	$\frac{5.668 \times 0.258 \times (1-0.258)}{(0.05)^2}$ = 434.05	440/55
EMC of V-I-S fraction images	$\frac{46318}{150605} = 0.308$	$\frac{5.454 \times 0.308 \times (1-0.308)}{(0.05)^2}$ = 465.0	469/67
EMC of V-S-Sh fraction images	$\frac{31022}{155744} = 0.204$	$\frac{5.668 \times 0.204 \times (1-0.204)}{(0.05)^2}$ = 368.18	376/47

It is noted that the total area of V-I-S fraction images is less than of the others because of its water area excluding.

One of the objectives of this study is to compare the accuracies of classification maps achieved from MLC and EMCs. The stratified sample points used for each class were randomly sampled according to number of locations summarized in Table 5.8. Reference data of those locations were used for accuracy assessment.

5.4.1 Accuracy assessments of MLC

1) Original Landsat5 TM images

Original Landsat5 TM images were classified into eight classes (Figure 5.7). The results of classification accuracy are presented in Table 5.9 and 5.10. From 384 of sample points, 257 are consistent to the reference data. The overall accuracy is 66.93% and overall Kappa statistic is 62.22%. Water presents the highest percentage of producer's and user's accuracies (94.00% and 97.92%, respectively). Horticultural area shows the lowest percentage of producer's accuracy (34.55%) and forest does for the lowest user's accuracy (37.50%).

Table 5.9 Error matrix of the LULC map derived from MLC of original Landsat5 TM images.

Class name	CBD	Residential	G/B	Shrub	Horticultural area	Forest	Paddy field	Water	Row total
CBD	25	10	10	1	1	0	0	1	48
Residential	2	46	0	0	0	0	0	0	48
G/B	0	3	40	0	3	0	2	0	48
Shrub	0	1	7	28	9	1	1	1	48
Horticultural area	0	3	16	8	19	0	1	1	48
Forest	0	0	5	13	12	18	0	0	48
Paddy field	0	0	3	0	11	0	34	0	48
Water	0	0	0	0	0	1	0	47	48
Column total	27	63	81	50	55	20	38	50	384

Table 5.10 Producer's and user's accuracies the LULC map derived from MLC of original Landsat5 TM images.

Class name	Reference total	Classified total	Number of consistency	Producer's accuracy	User's accuracy
CBD	27	48	25	92.59%	52.08%
Residential area	63	48	46	73.02%	95.83%
Grass field/ bare soil	81	48	40	49.38%	83.33%
Shrub	50	48	28	56.00%	58.33%
Horticultural area	55	48	19	34.55%	39.58%
Forest	20	48	18	90.00%	37.50%
Paddy field	38	48	34	89.47%	70.83%
Water	50	48	47	94.00%	97.92%
Total	384	384	257		

2) V-I-S fraction images

Fraction images of V-I-S combination were classified into seven classes (Figure 5.8). The results of classification accuracy are presented in Table 5.11 and 5.12. From 385 of sample points, 278 are consistent to reference data. The overall accuracy is 72.21% and overall Kappa statistic is 67.50%. CBD presents the highest percentage of producer's accuracy (100.00%) and the highest user's accuracy goes to residential (85.45%). Grass field/bare soil shows lowest percentage of producer's accuracy (54.22%) and forest does for the lowest user's accuracy (54.55%).

Table 5.11 Error matrix of the LULC map derived from MLC of V-I-S fraction images.

Class name	CBD	Residential	G/B	Shrub	Horticultural area	Forest	Paddy field	Row total
CBD	46	3	5	0	1	0	0	55
Residential	0	47	2	5	0	0	1	55
G/B	0	1	45	2	4	0	3	55
Shrub	0	2	4	41	7	0	1	55
Horticultural area	0	1	14	7	33	0	0	55
Forest	0	0	1	12	11	30	1	55
Paddy field	0	0	12	3	4	0	36	55
Column total	46	54	83	70	60	30	42	385

Table 5.12 The producer's and user's accuracies of the LULC map derived from MLC of V-I-S fraction images.

Class name	Reference total	Classified total	Number of consistency	Producer's accuracy	User's accuracy
CBD	46	55	46	100.00%	83.64%
Residential area	54	55	47	87.04%	85.45%
Grass field/ bare soil	83	55	45	54.22%	81.82%
Shrub	70	55	41	58.57%	74.55%
Horticultural area	60	55	33	55.00%	60.00%
Forest	30	55	30	100.00%	54.55%
Paddy field	42	55	36	85.71%	65.45%
Total	385	385	278		

3) V-S-Sh fraction images

Fraction images of V-S-Sh combination were classified into eight classes (Figure 5.9). The results of classification accuracy are presented in Table 5.13 and 5.14. From 440 of sample points, 295 are consistent to reference data. The overall accuracy is to 67.05% and overall Kappa statistic is 62.30%. Water presents the highest percentage of producer's and user's accuracies (98.15% and 96.36%, respectively). CBD shows the lowest percentage of producer's and user's accuracies (47.06% and 29.09%, respectively).

Table 5.13 Error matrix of the LULC map derived from MLC of V-S-Sh fraction images.

Class name	CBD	Residential	G/B	Shrub	Horticultural area	Forest	Paddy field	Water	Row total
CBD	39	8	3	3	2	0	0	0	55
Residen-tial	4	43	3	0	1	0	4	0	55
G/B	0	5	46	1	0	0	3	0	55
Shrub	0	0	6	42	7	0	0	0	55
Horticultural area	0	6	11	20	16	1	0	1	55
Forest	0	1	4	16	4	30	0	0	55
Paddy field	0	0	23	2	4	0	26	0	55
Water	1	0	0	1	0	0	0	53	55
Column total	44	63	96	85	34	31	33	54	440

Table 5.14 The producer's and user's accuracies of the LULC map derived from MLC of V-S-Sh fraction images.

Class name	Reference total	Classified total	Number of consistency	Producer's accuracy	User's accuracy
CBD	44	55	39	88.64%	70.91%
Residential area	63	55	43	68.25%	78.18%
Grass field/ bare soil	96	55	46	47.92%	83.64%
Shrub	85	55	42	49.41%	76.36%
Horticultural area	34	55	16	47.06%	29.09%
Forest	31	55	30	96.77%	54.55%
Paddy field	33	55	36	78.79%	47.27%
Water	54	55	53	98.15%	96.36%
Total	440	440	295		

5.4.2 Accuracy assessments of EMC

1) V-I-S fraction images.

Fraction images of V-I-S combination were classified into seven classes (Figure 5.10). The results of classification accuracy are presented in Table 5.15 and 5.16. From 469 of sample points, 321 are consistent to reference data. The overall accuracy is 68.44% and overall Kappa statistic is 63.20%. Residential presents the highest percentage of producer's accuracy (96.67%) and shrub presents the highest user's accuracy (97.01%). Paddy field shows the lowest percentage of producer's and user's accuracies (55.36% and 46.27%, respectively).

Table 5.15 Error matrix of the LULC map derived from EMC of V-I-S fraction images.

Class name	CBD	Residential	G/B	Shrub	Horticultural area	Forest	Paddy field	Row total
CBD	58	4	3	1	1	0	0	67
Residential	2	56	3	0	3	0	3	67
G/B	0	0	65	0	0	0	2	67
Shrub	0	12	5	42	5	0	3	67
Horticultural area	0	5	2	25	31	3	1	67
Forest	0	0	8	13	13	32	1	67
Paddy field	0	2	21	4	3	0	37	67
Column total	60	79	107	85	56	35	47	469

Table 5.16 The producer's and user's accuracies of the LULC map derived from EMC of V-I-S fraction images.

Class name	Reference total	Classified total	Number of correct	Producer's accuracy	User's accuracy
CBD	60	67	58	96.67%	86.57%
Residential area	79	67	56	70.89%	83.58%
Grass field/ bare soil	107	67	65	60.75%	97.01%
Shrub	85	67	42	49.41%	62.69%
Horticultural area	56	67	31	55.36%	46.27%
Forest	35	67	32	91.43%	47.76%
Paddy field	47	67	37	78.72%	55.22%
Total	469	469	321		

2) V-S-Sh fraction images

Fraction images of V-S-Sh combination were classified into eight classes (Figure 5.11). The results of classification accuracy are presented in Table 5.17 and 5.18. From 376 of sample points, 260 are consistent to reference data. The overall accuracy is 69.15% and overall Kappa statistic is 64.74%. Forest presents the highest percentage of producer's accuracy (93.55%) while water presents the highest user's accuracy (100.00%). Horticultural area shows the lowest percentage of producer's and user's accuracies (41.94% and 27.66%, respectively).

Table 5.17 Error matrix of the classification map derived from EMC of V-S-Sh fraction images.

Class name	CBD	Residential	G/B	Shrub	Horticultural area	Forest	Paddy field	Water	Row total
CBD	41	4	1	0	0	0	0	1	47
Residential	1	38	0	1	6	1	0	0	47
G/B	1	1	39	2	1	0	3	0	47
Shrub	0	0	4	37	5	0	1	0	47
Horticultural area	0	3	1	26	13	1	0	3	47
Forest	0	0	6	4	5	29	2	1	47
Paddy field	0	4	21	5	1	0	16	0	47
Water	0	0	0	0	0	0	0	47	47
Column total	43	50	72	75	31	31	22	52	376

Table 5.18 The producer's and user's accuracies of the LULC map derived from EMC of V-S-Sh fraction images.

Class name	Reference total	Classified total	Number of consistency	Producer's accuracy	User's accuracy
CBD	43	47	41	95.35%	87.23%
Residential area	50	47	38	76.00%	80.85%
Grass field/ bare soil	72	47	39	54.17%	82.98%
Shrub	75	47	37	49.33%	78.72%
Horticultural area	31	47	13	41.94%	27.66%
Forest	31	47	29	93.55%	61.70%
Paddy field	22	47	16	72.73%	34.04%
Water	52	47	47	90.38%	100%
Total	376	376	260		

CHAPTER VI

CONCLUSION AND DISCUSSION

6.1 Conclusion

For LULC classification, images from SMA have been proved to be more accurate than traditional TM images, particularly for heterogeneous area such as an urban or sub-urban (Lu and Weng, 2004). Therefore, this study aims at using LSMA to extract fraction images as additional data followed by EMC as an additional method to the conventional for classifying LULC of the urban area and the surrounding in Muang District, Nakhon Ratchasima Province. Results from the conventional and new methods applied to different sets of images were then evaluated how proper they were for LULC of the study area where considered different pattern characteristics from big towns of other regions in Thailand.

In this research, two types of classification methods, MLC which is considered to be the conventional and EMC, were applied to both original Landsat TM images and their derived fraction images. Two sets of fraction images which are V-I-S and V-S-Sh were extracted from the TM images using LSMA. While these four endmembers, vegetation, impervious surface, soil, and shade, were selected from scatter-plots of PCA images transformed from TM images. The MLC was used to classify original TM images, V-I-S and V-S-Sh fraction images. The EMC is a model represented by ternary diagram in which is separated to be LULC classes by the plots

of tremendous training data points. Each apex of ternary diagram is represented by an endmember which is a kind of earth surface cover. In this study, the EMC was applied to V-I-S and V-S-Sh fraction images. Two classification methods operating on three sets of images resulted in five LULC maps of the study area. The qualities of resultant classification maps were assessed in terms of overall, PA, and UA including Kappa statistics. These parameters were determined in error matrixes.

With original Landsat5 TM images and V-S-Sh fraction images, LULC of the study area was classified, using MLC, into eight classes, namely horticultural area, grass field/bare soil (G/B), forest, residential, CBD, shrub, paddy field, and water. While became seven classes excluding water when V-I-S fraction images were used to classify. For EMC, the training data points/pixels of each set of fraction images (V-I-S and V-S-Sh) were input to CSpace1.01 software to define composition limits of three components for each LULC class. Then, the diagrams with LULC class limits were used as templates to classify LULC of unknown data points/pixels. Percentage of each LULC class in each classification map derived from different methods is listed in Table 6.1

The number of sample points of each class for error analysis was calculated by use of the multinomial distribution function. Stratified sample points method of software ERDAS was used to locate points randomly sampled for accuracy assessment of each map. Field data and aerial photographs were used as references to verify accuracy of those points which in turn indicated accuracy of each class a overall accuracy of each map. The overall accuracy and overall Kappa statistics of maps classified from three sets of images by two different methods were concluded in Table

6.2. PA and UA were estimated for each class of those five maps as shown in Table 6.3.

Table 6.1 Summarized percentage of each LULC class from each map of different classification methods.

Classification method of images	CBD	Residential area	G/B	Shrub	Horticultural area	Forest	Paddy field	Water
MLC of original TM	16.1%	21.3%	12.2%	18.2%	7.6%	3.8%	18.5%	2.2%
MLC of V-I-S	12.0%	22.4%	13.9%	18.3%	12.7%	11.4%	9.3%	-
MLC of V-S-Sh	11.9%	15.0%	25.8%	17.1%	25.8%	9.3%	7.3%	2.4%
EMC of V-I-S	8.8%	14.4%	6.1%	18.4%	30.8%	14.2%	7.4%	-
EMC of V-S-Sh	7.9%	20.4%	11.5%	13.5%	14.5%	13.3%	17.4%	1.4%

Table 6.2 Summarized overall accuracy and overall Kappa statistics of each map classified using different sets of images and methods

Classification method and set of images	Overall accuracy	Overall Kappa statistics
MLC of original TM	66.93%	62.20%
MLC of V-I-S	72.21%	67.50%
MLC of V-S-Sh	67.05%	62.30
EMC of V-I-S	68.44%	63.20
EMC of V-S-Sh	69.15%	64.70

Table 6.3 Summarized PA and UA of each LULC class for all classification methods

Classification method	CBD	Residential area	G/B	Shrub	Horticultural area	Forest	Paddy field	Water
MLC of original TM								
- PA	92.59%	73.02%	49.38%	56.00%	34.55%	90.00%	89.47%	94.00%
- UA	52.08%	95.83%	83.33%	58.33%	39.58%	37.50%	70.83%	97.92%
MLC of V-I-S								
- PA	100.00%	87.04%	54.22%	58.57%	55.00%	100.00%	85.71%	-
- UA	83.64%	85.45%	81.82%	74.55%	60.00%	54.55%	65.45%	-
MLC of V-S-Sh								
- PA	88.64%	68.25%	47.92%	49.41%	47.06%	96.77%	78.79%	98.15%
- UA	70.91%	78.18%	83.64%	76.36%	29.09%	54.55%	47.27%	96.36%
EMC of V-I-S								
- PA	96.67%	70.89%	60.75%	49.41%	55.36%	91.43%	78.72%	-
- UA	86.57%	83.58%	97.01%	62.69%	46.27%	47.76%	55.22%	-
EMC of V-S-Sh								
- PA	95.35%	76.00%	54.17%	49.33%	41.94%	93.55%	72.73%	90.38%
- UA	87.23%	80.85%	82.98%	78.72%	27.66%	61.70%	34.04%	100%

6.2 Discussion

Results from different combinations of sets of images and operations of classifications are discussed herein. A percentage of classified LULC is summarized in Table 6.1. Residential area, shrub, CBD, and G/B almost equally share main part of the study area followed by considering not small parts of horticultural area and less paddy field and forest. This implies that this study area is not ordinary urban because in general urban area will consist obviously more of CBD and residential area than other types. Therefore, the discussion on accuracy of maps will be focused more at CBD and residential area which should be major part of any urban. G/B and shrub could be considerable parts in any developing urban too.

From Table 6.2, all maps derived from fraction images show higher overall accuracy and Kappa statistics than the one from original TM images. This can confirm that fraction images obtained from LSMA model carry higher potential than the TM images in applying to LULC classification. MLC of V-I-S combination shows the highest accuracy. MLC of TM images show the lowest. However, different combinations of methods and fraction images show no obvious difference in overall accuracy and Kappa statistics. Conclusively, V-I-S combination shows hardly higher accuracy than V-S-Sh. MLC also shows hardly higher accuracy than EMC.

The accuracy, based on producer and user, of a classified LULC map is dependent of image type and classification method. From Table 6.3, accuracy comparison of some classes is discussed according to different classification methods and sets of images used. These classes are CBD, residential area, G/B, and shrub which are more related to urban.

1) CBD - MLC of V-I-S, EMC of V-I-S, and EMC of V-S-Sh provide almost the same accuracy for this class. MLC of V-I-S provides 100% of PA and 83.64% of UA. It means that, using MLC, V-I-S fraction images can keep characteristics of this unit so well that all areas of the class is classified but still carry other classes' characteristic similar to this class as much as 16.36%. While EMC of V-S-Sh provides the highest UA (87.23%). It means that V-S-Sh is the best among types of image in terms of least carrying other classes' characteristic that is similar to this class (12.77%).

2) Residential area - MLC of V-I-S, MLC of TM, EMC of V-S-Sh, and EMC of V-I-S provide more to less accuracy to this unit respectively. MLC of V-I-S provides the best PA (87.04%) and 85.45% UA. It means that, using MLC, V-I-S fraction images are the best to keep characteristics of this unit so well that only 12.96% of this unit is misclassified but still carry other classes' characteristic similar to this class as much as 14.55%. While MLC of TM provides the best UA (95.83%). It means that, using MLC, TM is the best among types of image in terms of least carrying other classes' characteristic that is similar to this class (only 4.17%).

3) G/B - EMC of V-I-S provides outstanding higher accuracy to this unit than others which are about the same. This combination also provides the best PA (60.75%) and UA (97.01%). It means that, using EMC, V-I-S fraction images are the best to keep characteristics of this unit so well that 39.25% of this unit is misclassified and carry other classes' characteristic similar to this class only 2.99%.

4) Shrub – MLC of V-I-S provides higher accuracy than others, followed by EMC of V-S-Sh and MLC of V-S-Sh. MLC of V-I-S provides the best PA (58.57%) and 74.55% UA. It means that, using MLC, V-I-S fraction images are the best to keep

characteristics of this unit so well that 41.43% of this unit is misclassified but still carry other classes' characteristic similar to this class as much as 25.45%. While EMC of V-S-Sh provides the best UA (78.72%). It means that, using EMC, V-S-Sh is the best among types of image in terms of least carrying other classes' characteristic that is similar to this class (21.28%).

From above discussion, V-I-S fraction images show more accuracy when applying to urban classification than V-S-Sh set. Nevertheless, the accuracy achieved from this study is still lower than ones of other researches using the same method such as the one of Lu and Weng (2004) of which overall accuracy can reach to 89.33%. The significant difference between this research and others could be the characteristics of study areas. Most researchers used metropolitan city as study areas such as Indianapolis (Lu and Weng, 2004; Lu and Weng, 2006) and metropolitan of Columbus Ohio (Wu and Murray, 2002; Wu, 2004). Those study areas have well systematic development and zonal management. Their CBDs are always located as the centers which are clearly separated from other classes. Residential areas are also developed clearly as zones. In contrast, in Nakhon-Ratchasima municipal area, residential areas are always mixed with CBD, industrial and even horticultural area. This can result in decreasing the classification accuracy.

From this study, it is found that endmember selection is needed to be improved because RMSEs are too high (2.16 for V-I-S and 2.38 for V-S-Sh) compared with other researches. According to Wu (2004), the brightness normalization method was applied to reduce brightness variation of images. This could help increase ability in selecting pure endmember signatures more precisely. Additionally, to increase accuracy of LULC classification, census data could be used to incorporate with the

LSMA method (Lu and Weng, 2006). These two additional techniques are here recommended for further study.

REFERENCES

REFERENCES

- Adams, J. B., Sabol, D.E., Kapos, V., Filho, R.A., Roberts D.A., Smith, M.O., and Gillespie, A.R. (1995). Classification of Multispectral Image Base on Fraction Endmembers: Application to land Cover Change in The Brazilian Amazon. **Remote Sensing of Environment**. 52: 137-154.
- Adam, J.B., Smith, M.O., and Johnson, P.E. (1986). Spectral Mixture Modeling; A New Analysis of Rock and Soil Types at the Viking Lander 1 Site. **Journal of Geographical Research**. 91: 8098-8122.
- Bajjouk, T., Populus, J., and Guillaumont, B. (1998). Quantification of Subpixel Cover Fractions Using Principal Component Analysis and a Linear Programming Method: Application to the Coastal Zone of Roscoff (France). **Remote Sensing of Environment**. 64: 153-165.
- Bateson, A., and Curtiss, B. (1996). A Method for Manual Endmember Selection and Spectral Unmixing. **Remote Sensing of Environment**. 55: 229-243.
- Chunfang, K., Kai, X., and Chonglong, W. (2006). Classification and Extraction of Urban Land-Use Information from High-Resolution Image Based on Object Multi-Features. **Journal of China University of Geosciences**. 17: 151-157.
- Cleve, C., Kelly, M., Kearns, F., and Moritz, M. (2008). Classification of the Wildland-Urban Interface: A Comparison of Pixel and Object based Classifications Using High-Resolution Aerial Photography. **Computer, Environment and Urban Systems**. Article in press.

- Defries, R. S., Hansen, M. C., and Townshend, J. R. G. (2000). Global Continuous Fields of Vegetation Characteristics: a Linear Mixture Model Applied to Multi- Year 8 km. AVHRR Data. **International Journal of Remote Sensing**. 21(6&7): 1389-1414.
- Dumas, E., Jappiot, M., and Tatoni, T. (2008). Mediterranean Urban-Forest Interface Classification (MUFIC): A Quantitative method combining SPOT 5 Imagery and Landscape Ecology Indices. **Landscape and Urban Planning**. 84: 183-190.
- Friedl, M.A., and Brodley, C.E. (1997). Decision Tree Classification of Land Cover from Remotely Sensed Data. **Remote Sensing of Environment**. 61: 399-409.
- Guindon, B., Zhang, Y., Dillabaugh, C. (2004). Landsat Urban Mapping Based on a Combined Spectral-Spatial Methodology. **Remote Sensing of Environment**. 92: 218-232.
- Han, D., Chao, W.R., Ping, W.J., Bin, Z., Zhou, S., and Xia, D.L. (2004). Quantifying Land Use Change in Zhejiang Coastal Region, China Using Multi-Temporal Landsat TM/ETM+ Images. **Soil Science Society of China**. 17(6): 712-720.
- Jensen, J. R. (2005). **Introductory Digital Image Processing: A Remote Sensing Perspective** (3rd ed.). USA: Prentice Hall.
- Jensen, L.M. (1997). Classification of Urban Land Cover Based on Expert Systems, Object Models and Texture. **Computer, Environment and Urban System**. 21: 291-302.

- Ju, J., Koczaczyk, D. E., and Gopal, S. (2003). Gaussian Mixture Discriminant Analysis and Sub Pixel Land Cover Characterization in Remote Sensing. **Remote Sensing of Environment**. 84: 550-560.
- Kandrika, S., and Roy, P.S. (2008). Land Use Land Cover Classification of Orissa Using Multi-Temporal IRS-P6 Awifs Data: A Decision Tree Approach. **International Journal of Applied Earth Observation and Geoinformation**. 10: 186-193
- Kardi, T. (2007). Remote Sensing of Urban Areas: Linear Spectral Unmixing of Landsat Thematic Mapper Images Acquired Over Tartu (Estonia). **Proc. Estonian Acad. Sci. Biol. Ecol**. 56(1): 19-32.
- Kaya, S., and Curran, P.I, (2006). Monitoring Urban Growth on the European Side of the Istanbul Metropolitan Area: A Case Study. **International Journal of Applied Earth Observation and Geoinformation**. 8: 18-25.
- Leica Geosystems. (2002). **ERDAS Field Guide. Sixth Edition**. USA.
- Leica Geosystems. (2002). **ERDAS IMAGINE Tour Guides**. USA.
- Lu, D., and Weng, Q. (2004). Spectral Mixture Analysis of the Urban Landscape in Indianapolis City With Landsat ETM⁺ Imagery. **Photogrammetric Engineering & Remote Sensing**. 70(9): 1053-1062.
- Lu, D., and Weng, Q. (2006). Use of Impervious Surface in Urban Land-Use Classification. **Remote Sensing of Environment**. 102: 146-160.
- Lu, D., Moran, E., and Batistella, M. (2003). Linear Mixture Model Applied to Amazon Vegetation Classification. **Remote Sensing of Environment**. 87: 456-469.

- Matthias, B., and Martin, H. (2003). Mapping Imperviousness Surface Using NDVI and Linear Spectral Unmixing of ASTER Data in the Cologne- Bonn Region (Germany). In **Proceedings of the SPIE 10th International Symposium on Remote Sensing 2003**. Barcelona, Spain.
- Mcnairn, H., Deguise, J. C., Pacheco, A. Shang, J., and Rabe, N. (2001). Estimation of Crop Cover and Chlorophyll from Hyperspectral Remote Sensing. **23th Canadian Remote Sensing Symposium**. Sainte-Ioy Quebec, Canada.
- Painter, T. H., Dezier, J., Roberts, D. A., Davis, R. E., and Green, R. E. (2003). Retrieval of Subpixel Snow-Cover Area and Grain Size from Imaging Spectrometer Data. **Remote Sensing of Environment**. 85: 64-87.
- Plaza, A., Martínez, P., Pérez, R., and Plaza, J. (2002). Spatial/Spectral Endmember Extraction by Multidimensional Morphological Operations. **IEEE Transactions on Geoscience and Remote Sensing**. 40(9): 2025-2041.
- Powell, R.B., Roberts, D.A., Denison, P.E., and Hess, L.L. (2007). Sub-Pixel Mapping of Urban Land Cover Using Multiple Endmember Spectral Mixture Analysis: Manaus, Brazil. **Remote Sensing of Environment**. 106: 253-267.
- Ridd, M.K. (1995). Exploring a V-I-S (Vegetation- Impervious surface- Soil) Model for Urban Ecosystem Analysis through Remote Sensing: Comparative Anatomy for Cities. **International Journal of Remote Sensing**. 16: 2165-2185.
- Ridd, M.K., and Chung, J.J. (1990). Sub-Pixel Analysis of SPOT Satellite Data in an Urban Environment. **Paper Presented at the Association of America Geographers Manual Meeting**, Toronto, Canada, 19-22 April, 1990.

- Sabol, D.E., Gillespie, A.R., Adam, J. B., Smith, M. O., and Tucker, C. J. (2002). Structural State in Pacific Northwest Forests Estimated Using Simple Mixture Model of Multispectral Images. **International Journal of Remote Sensing**. 80: 1-16.
- Small, C. (2001). Estimation of Urban Vegetation Abundance by Spectral Mixture Analysis. **International Journal of Remote Sensing**. 22: 1305-1334.
- Small, C. (2003). High Spatial Resolution Spectral Mixture Analysis of Urban Reflectance. **Remote Sensing of Environment**. 88: 170-186.
- Small, C. (2004). The Landsat ETM+ Spectral Mixing Space. **Remote Sensing of Environment**. 93: 1-17.
- Small, C., and Lu, J.W.T. (2006). Estimation and Vicarious Validation of Urban Vegetation Abundance by Spectral Mixture Analysis. **Remote Sensing of Environment**. 100: 441-456.
- Stefanov, W.L., Ramsey, M.S., and Christensen, P.R. (2001). Monitoring Urban Land Cover Change: An Expert System Approach to Land Cover Classification of Semiarid to Arid Urban Centers. **Remote Sensing of Environment**. 77: 173-185.
- Weng, Q., Lu, D., and Schubring, J. (2004). Estimation of Land Surface Temperature-Vegetation Abundance Relationship for Urban Heat Island Studies. **Remote Sensing of Environment**. 89: 467-483.
- Weydahl, D.J., Bretar, F., and Bjerke, P. (2005). Comparison of RADARSAT-1 and IKONOS Satellite Images for Urban Features Detection. **Information Fusion**. 6: 243-249.

- Wu, C. (2004). Normalized Spectral Mixture Analysis for Monitoring Urban Composition Using ETM⁺ Imagery. **Remote Sensing of Environment**. 93: 480-492.
- Wu, C., and Murray, A.T. (2003). Estimating Impervious Surface Distribution by Spectral Mixture Analysis. **Remote Sensing of Environment**. 84: 493-505.
- Yuan, F., Saway, K.E., Loeffelholz, B.C., and Bauer, M.E. (2005). Land Cover Classification and Change Analysis of the Twin Cities (Minnesota) Metropolitan Area by Multitemporal Landsat Remote Sensing. **Remote Sensing of Environment**. 89: 317-328.
- Zhu, G., and Blumberg, D.G. (2002). Classification Using ASTER Data and SVM Algorithms; the Case Study of Beer Sheva, Israel. **Remote Sensing of Environment**. 80: 233-240.

CURRICULUM VITAE

CHOTIPA KULRAT

Gender: Female

Nationality: Thai

Date of birth: July 20, 1978

Education background:

1998-2001 Bachelor Degree of Science in Physic, Thammasat University, Thailand

Presentation:

Kulrat, C., and Sarapirome, S. (2006). Land-Use Classification of the Great City of

Nakhon Ratchasima Using Linear Spectral Mixture Analysis. **National**

Conference on Mapping and Geo-Informatics. Ambassador City Jomtien

Hotel, Chonburi Province, Thailand.